Research Paper

GEOSPHERE

GEOSPHERE, v. 19, no. 2

https://doi.org/10.1130/GES02583.1

14 figures; 1 supplemental file

CORRESPONDENCE: jning027@uottawa.ca

CITATION: Ningthoujam, J., Arnott, R.W.C., and Wearmouth, C., 2023, Systematic vertical organization of matrix-rich and associated matrix-poor sandstones in ancient deep-marine slope and basin-floor deposits: Geosphere, v. 19, no. 2, p. 558–582, https://doi.org/10.1130/GES02583.1.

Science Editor: David E. Fastovsky
Associate Editor: Andrea Fildani

Received 9 August 2022
Revision received 13 November 2022
Accepted 8 December 2022

Published online 27 February 2023

Systematic vertical organization of matrix-rich and associated matrix-poor sandstones in ancient deep-marine slope and basin-floor deposits

Jagabir Ningthoujam[1,2], R.W.C. (Bill) Arnott[1], and Curran Wearmouth[1,3]

[1]Department of Earth and Environmental Sciences, University of Ottawa, Ottawa, Ontario K1N 6N5, Canada
[2]Canadian Natural Resources Ltd., 855 2 Street SW, Calgary, Alberta T2P 4J8, Canada
[3]British Columbia Geological Survey, 1810 Blanshard Street, Victoria, British Columbia V8T 4J1, Canada

ABSTRACT

Deep-marine two-part strata consisting of a sand-rich basal part overlain sharply by a mud-rich upper part have been termed linked debrites, hybrid event beds, transitional flow deposits, and bipartite facies. In continental slope and proximal basin floor strata of the Neoproterozoic Windermere Supergroup (western North America) and distal basin-floor strata of the Ordovician Cloridorme Formation (eastern North America), bipartite facies form the middle of a depositional continuum hundreds of meters long consisting upflow of thick-bedded, matrix-poor sandstone (<20% detrital mud matrix) to thin-bedded, sandy mudstone (50%–90% mud matrix). This consistent lithofacies change is interpreted to reflect particle settling in a rapidly but systematically evolving, negligibly sheared sand-mud suspension developed along the margins (Windermere) and downflow terminus (Cloridorme) of a high-energy, mud-enriched avulsion jet.

In both study areas, beds of similar lithofacies type succeed one another vertically and transform to the next facies in the depositional continuum at about the same along-strike position, forming stratal units two to nine beds thick whose grain-size distribution gradually decreases upward. This spatial and temporal regularity is interpreted to be caused by multiple surges of a single, progressively waning turbidity current, with sufficient lag between successive surges for the deposition of a traction-structured sandstone overlain by mudstone cap. Furthermore, the systematic back-stepping or side-stepping recognized at the stratal unit scale is interpreted to have been driven by a combination of knickpoint migration and local topographic steering of the flows, which continued until the supply of mud from local seafloor erosion became exhausted, the main channel avulsed elsewhere, or a new stratal element developed.

INTRODUCTION

Deep-marine matrix-rich (>20% clay and silt content) strata that are unlike classical turbidites (*sensu* Bouma, 1962; Lowe, 1982) or debrites have been increasingly recognized in both modern and ancient turbidite systems (e.g., Lowe and Guy, 2000; Haughton et al., 2003, 2009; Hodgson, 2009; Kane and Pontén, 2012; Talling, 2013; Terlaky and Arnott, 2014). Termed slurry beds (Lowe and Guy, 2000), linked debrites (Haughton et al., 2003), co-genetic debrite-turbidite beds (Talling et al., 2004), hybrid event beds (Haughton et al., 2009), transitional flow deposits (Kane and Pontén, 2012), and bipartite facies (Angus et al., 2019), these strata typically consist of a sandy basal part overlain sharply by a muddier, mud clast–bearing upper part, with the contact being either planar (e.g., Haughton et al., 2009; Talling, 2013; Pierce et al., 2018) or irregular (e.g., Haughton et al., 2009; Patacci et al., 2014; Fonnesu et al., 2015, 2016, 2018; Southern et al., 2015), or less commonly gradational and marked by an intervening unit of alternating light (mud-poor) and dark (mud-rich) colored bands (e.g., Barker et al., 2008; Davis et al., 2009; Pierce et al., 2018). Additionally, these composite strata are reported to occur downflow of clean (i.e., less mud-rich) sand and upflow of argillaceous (i.e., mud-rich) sand over distances of hundreds of meters to tens of kilometers in what has been interpreted to be an along-flow proximal-to-distal depositional continuum (e.g., Fonnesu et al., 2015, 2016, 2018; Kane et al., 2017; Spychala et al., 2017a; Pierce et al., 2018; Angus et al., 2019; Ningthoujam et al., 2022). The central focus of these studies has been aimed largely at understanding either the physical origin of the composite strata at the individual bed scale (e.g., Davis et al., 2009; Haughton et al., 2009; Baas et al., 2011; Talling, 2013; Fonnesu et al., 2015, 2016; Angus et al., 2019; Koo et al., 2020) or their stratigraphic and geographic distribution at the stratal element scale (several-meters-thick stratal package comprising two or more event beds and in which >50% of the beds are composed of a single sedimentary facies) (e.g., Haughton et al., 2009; Kane and Pontén, 2012; Patacci et al., 2014; Terlaky and Arnott, 2016; Kane et al., 2017; Spychala et al., 2017b; Pierce et al., 2018). Lacking, however, is an in-depth discussion of how these beds stack vertically and therefore how the sedimentological conditions that deposited them changed in time. Accordingly, this study describes the vertical stacking character and spatial pattern of matrix-rich and associated matrix-poor lithologies observed at the bed and stratal unit scales in slope and proximal basin-floor deposits of the Neoproterozoic Windermere turbidite system (western North America) and

Jagabir Ningthoujam https://orcid.org/0000-0001-5058-8533

distal basin-floor deposits of the Ordovician Cloridorme Formation (eastern North America). Stacking patterns derived from field-based observations are then evaluated using a first-order Markov chain (e.g., Krumbein, 1968; Carr, 1982; Davis, 1986) to quantitatively determine whether there is any systematic stacking arrangement, and if so, identify possible physical drivers responsible for the pattern. This statistical technique has previously been applied to describe and interpret deep-marine matrix-rich strata at either the individual bed scale (e.g., Lowe and Guy, 2000; Haughton et al., 2003; Davis et al., 2009) or the stratal element scale (e.g., Kane and Pontén, 2012; Terlaky and Arnott, 2016); however, in this study, Markov chain analysis is carried out to assess the stacking patterns of beds and stratal units of matrix-rich and associated matrix-poor lithologies, and this study therein attempts to address the gap in understanding that remains between the deposition of an individual bed and that of a stratal element.

GEOLOGICAL BACKGROUND

Windermere Supergroup

The Neoproterozoic (740–570 Ma) Windermere Supergroup (WSG) is an unconformity-bounded succession of mostly metasedimentary rocks deposited on the passive continental margin of Laurentia (ancestral North America) during the breakup of the Rodinia supercontinent (Stewart, 1972; Ross and Arnott, 2007; McMechan, 2015). The outcrop belt of the WSG stretches from northwestern Mexico through the western United States and Canada and northward to the Yukon-Alaska border (Ross and Arnott, 2007) (Fig. 1A). In the southern Canadian Cordillera, the basal rift sequence includes a few-kilometers-thick assemblage of intercalated glacial diamictites and mafic volcanic rocks of the Toby and Irene Formations, respectively (Aalto, 1971; Ross et al., 1995; Warren, 1997). This is then overlain by a 5–7-km-thick post-rift, upward-shoaling succession composed of deep-marine basin floor (Kaza Group) followed by continental slope (Isaac Formation) to upper continental slope and shelf (Cunningham and Yankee Belle Formations, respectively) deposits (Campbell et al., 1973).

Deep-marine strata of the WSG basin (Fig. 1B), termed the Windermere turbidite system, are well exposed throughout the southern Canadian Cordillera (Fig. 1A). At the Castle Creek study area (Fig. 1D), vertically dipping, recently deglaciated, vegetation-free strata of the Upper Kaza Group and Isaac Formation form an outcrop belt that is ~2.6 km thick and 8 km wide (Terlaky et al., 2016; Navarro and Arnott, 2020). Here, field observations of beds and bedsets can be carried out over distances of tens of meters vertically, but more significantly, hundreds of meters along the strike of the outcrop. However, due to the two-dimensionality of the outcrop, paleoflow data are limited to a small number of well-exposed three-dimensional current ripples and dune cross-stratified sets and a small number of flute marks, which collectively indicate a general transport direction ranging from west-northwest to northeast (see Ross and Arnott, 2007; Schwarz and Arnott, 2007; Khan and Arnott, 2011; Navarro and Arnott, 2020) and therefore subparallel to the regional paleoflow direction (e.g., Mountjoy and Aitken, 1963).

Furthermore, rocks in the study area have undergone low-grade (greenschist facies) metamorphism, resulting in the alteration of primary clay matrix to muscovite and chlorite and strain-induced structures like bulging recrystallization and sub-grain rotation along some grain boundaries. Despite these changes, primary sedimentary structures and most sedimentary textures, namely grain size, grain shape, and sorting, are well preserved, enabling these rocks to be described and classified as sedimentary rocks (Ross and Arnott, 2007; Ningthoujam et al., 2022).

Cloridorme Formation

The Middle Ordovician (460–445 Ma) Cloridorme Formation (CF) comprises the Quebec segment of a succession of turbidite systems that were deposited along an elongate foreland basin located between cratonic North America to the northwest and the developing Taconic orogen and its associated volcanic arcs to the southeast (St. Julien and Hubert, 1975; Hiscott et al., 1986). The basin extended from Newfoundland (eastern Canada) to Tennessee (eastern United States) and was as much as 150 km wide (Hiscott, 1984). The CF is exposed semi-continuously for ~150 km along the north shore of the Gaspé Peninsula, Quebec, Canada (Fig. 1A). The CF is at least 4 km thick and, based on lithofacies and extensive marker beds (megaturbidites), is divided, from oldest to youngest, into five members: Saint Hélier member, composed of distal basin-floor mudstones; Pointe-à-la-Frégate and Petite-Vallée members, consisting of sandstone-rich lobe and mudstone-rich inter-lobe deposits; Mont-Saint-Pierre member, made up of distal basin-floor mudstones; and Marsoui member, made up of sand lobes and inter-lobe deposits (Hiscott et al., 1986) (Fig. 1C). This study focuses on strata of the Petite-Vallée member located near the village of Petite Vallée, Quebec (Fig. 1E). Here, strata are nearly vertically dipping (average 78°) and east-to-west (271°) striking and exposed along an intertidal wave-cut platform that allowed for field observations of beds and bedsets to be carried out over tens of meters vertically but also tens to hundreds of meters along the strike of the outcrop. In the study area, average paleocurrent based on base-of-bed tool and flute marks and troughs of three-dimensional current ripples is 272° (n = 102) and therefore sub-parallel to the strike of the outcrop, which is consistent with previous studies in other parts of the CF (Parkash and Middleton, 1970; Pickering and Hiscott, 1985; Awadallah, 2002). Rocks in the study area have experienced very low-grade (zeolite to prehnite-pumpellyite facies) metamorphism associated with the Taconic orogeny and resulted in the alteration of primary clay minerals to illite and chlorite (Jiang and Peacor, 1994). Despite this change, primary sedimentary structures and textures are well preserved, allowing these strata to be described and classified using conventional sedimentary terminology (see Ningthoujam et al., 2022).

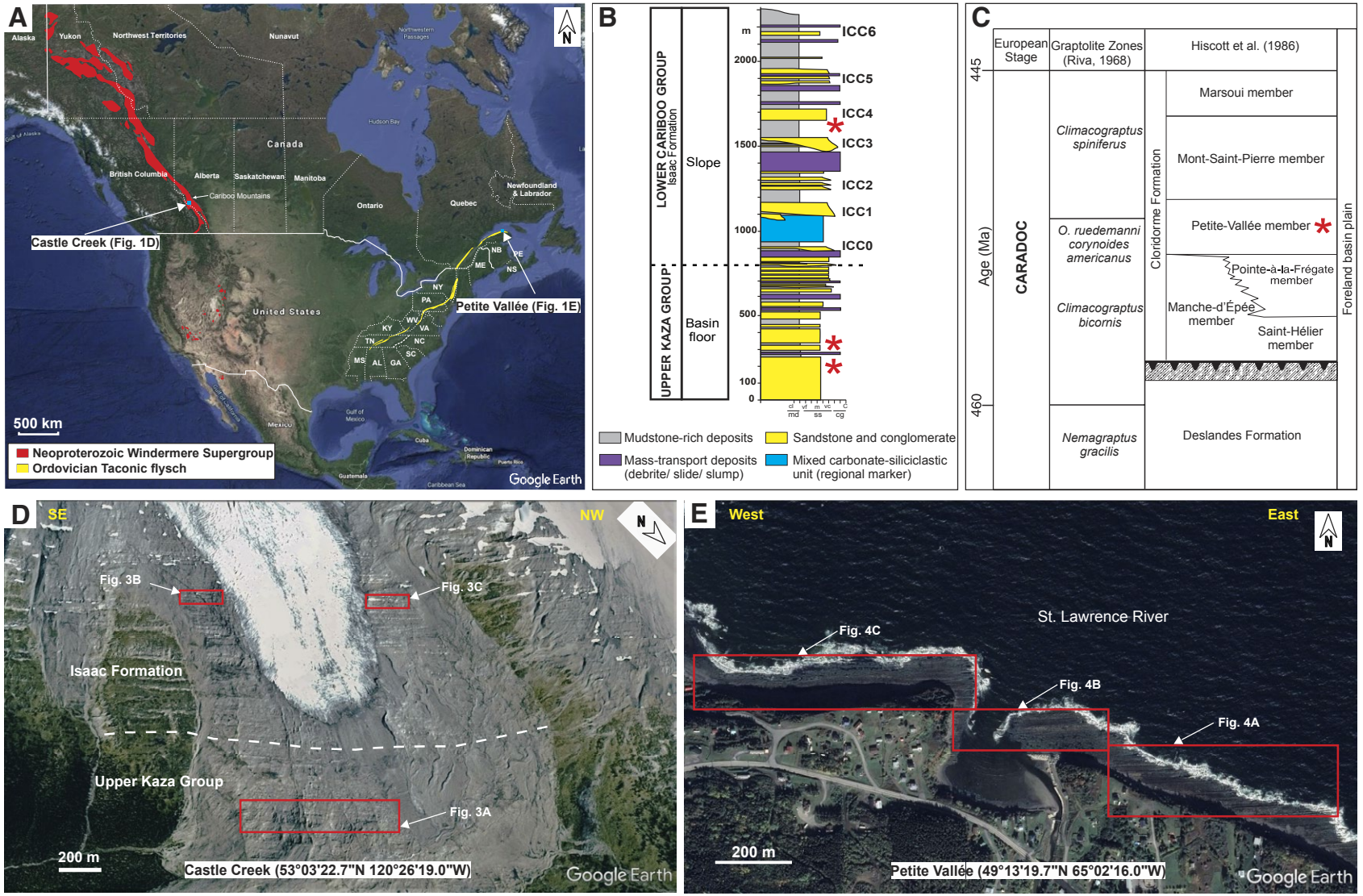

Figure 1. (A) Map of North America showing distribution of Windermere Supergroup (red) and Ordovician Taconic flysch (yellow) rocks. Study areas (Castle Creek and Petite Vallée) are indicated by blue squares (satellite image from Google Earth). (B) Windermere stratigraphy at Castle Creek study area. Here, basin-floor strata of the Upper Kaza Group are conformably overlain by continental slope deposits of the Isaac Formation. Informal names for Isaac slope channel complexes are numbered from ICC0 to ICC6. Locations of study intervals are indicated by red stars. Grain-size abbreviations: md—mudstone, ss—sandstone, cg—conglomerate, cl—clay, vf—very fine sand, m—medium sand, vc—very coarse sand, c—cobble. (C) Stratigraphy of the Middle Ordovician Cloridorme and Deslandes Formations in southeastern Quebec. Red star indicates location of the interval described in this study. (D) Castle Creek study area in the Cariboo Mountains, east-central British Columbia, Canada (satellite image from Google Earth). Note that strata are vertically dipping and recently deglaciated. Red rectangles indicate the study intervals. (E) Overview of study area located in the village of Petite Vallée, Quebec, Canada (satellite image from Google Earth). Strata are exposed along a broad wave-cut platform and are overturned, dipping south at 65°– 88°. Study intervals are indicated by red rectangles (after Ningthoujam et al., 2022).

PREVIOUS WORK—ALONG-STRIKE FACIES CHANGES

In slope and proximal basin-floor deposits of the WSG and distal basin-floor deposits of the CF, four main lithofacies linked with matrix-rich and associated matrix-poor strata were recognized (Terlaky and Arnott, 2014; Angus et al., 2019; Ningthoujam et al., 2022). Based on matrix content, the four lithofacies are: matrix-poor sandstone (MPS) with 0%–20% matrix content; muddy sandstone (MS) with 20%–50% matrix content; bipartite facies (BF) with a basal sandy (30%–60% matrix) part overlain sharply by a planar- to irregular-based muddier upper part (40%–80% matrix); and sandy mudstone (SM) with 50%–90% matrix content (Fig. 2). All four facies are structureless (i.e., lack tractional sedimentary structures), massive or coarse-tail graded, and composed of rounded to angular, equant to elongate framework grains that range from very fine to very coarse sand. Mud and lesser very fine- to medium-grained sandstone clasts are also common. Clasts are typically elongate, sub-angular to sub-rounded, and oriented with their maximum projection plane sub-parallel to bedding. Where present, these strata are then capped by lamina to thin beds of traction-structured sandstone overlain by silty mudstone. Tracing of individual beds along the strike of the outcrop in the WSG (Terlaky and Arnott, 2014; Angus et al., 2019; Wearmouth, 2018; Ningthoujam et al., 2022) and CF (Ningthoujam et al., 2022) reveals a systematic arrangement of lithofacies, namely, MPS to MS to BF and then to SM, each overlain, except where eroded, by a laminated to thin-bedded, traction-structured sandstone and silty mudstone (Fig. 2). More specifically, thick-bedded MPS gradually transforms to medium- to thick-bedded MS, which then develops into medium-bedded two-part BF consisting of a basal muddy sandstone overlain sharply by an upper sandy mudstone commonly containing dispersed mud clasts. Further along the transect, the basal part of BF progressively thins and then pinches out, whereas the upper part thickens but at a diminishing rate. Further laterally, following the termination of the basal sandy part of BF, the now exclusively SM thins to a pinch-out (Fig. 2). Importantly, these changes occurred over a horizontal distance of a few hundreds of meters and were interpreted to reflect a downflow (proximal to distal) depositional continuum, which in the WSG was interpreted to be oriented at a high angle to the main flow (Terlaky and Arnott, 2014; Wearmouth, 2018; Angus et al., 2019; Ningthoujam et al., 2022) but more or less parallel to the main flow in the CF (Ningthoujam et al., 2022). Significantly, regardless of the orientation of the depositional transect (parallel or at high angle) to the main flow or of depositional setting (continental slope versus proximal or distal basin floor), the transitions from MS to BF, BF to SM, and SM to its pinch-out were reported to be of proportionate length (Ningthoujam et al., 2022) and, accordingly, suggest similarity in depositional process.

Based on field observations, matrix-rich and associated matrix-poor strata stack exclusively to form stratal elements several meters to tens of meters thick that typically underlie sand-rich stratal elements such as slope channels, distributary channels, and terminal splays in the continental slope to proximal basin floor settings of the WSG (Terlaky and Arnott, 2014; Terlaky et al., 2016; Angus et al., 2019; Ningthoujam et al., 2022) (e.g., Fig. 3) and sandy terminal splays in the distal basin floor setting of the CF (Ningthoujam et al., 2022) (e.g., Fig. 4). This stratigraphic relationship was attributed to avulsion, and the stratal elements were identified as "avulsion splays" (*sensu* Terlaky and Arnott, 2014). Avulsion formed high-energy, momentum-driven turbulent wall jets that eroded the mud-rich inter-channel area and charged the flow with fine-grained sediment, namely very fine sand to clay, in addition to low-density mud clasts (Arnott, 2007a, 2007b; Terlaky and Arnott, 2014; Angus et al., 2019; Navarro and Arnott, 2020; Ningthoujam et al., 2022). The local incorporation of easily suspended fine-grained sediment resulted in an abrupt increase in local effective viscosity and a dramatic change in the characteristics and reduction in the diffusion of turbulence required to maintain the particle suspension. This caused the sediment suspension to rapidly exceed transport capacity and collapse, forming a negligibly sheared suspension that deposited a systematic along-flow depositional continuum consisting of MPS to MS to BF and then SM over distances of hundreds of meters. Following the emplacement of the depositional continuum from the collapsed suspension, a remnant low-density turbidity current reworked the top of the deposit and formed a thin-bedded, very fine-grained, upper-division turbidite capped by a silty mudstone deposited by a gelled near-bed fluid-mud layer. In continental slope and proximal basin-floor deposits of the WSG, the depositional transect developed along the margins of the high-energy wall jet, whereas in the distal basin-floor setting of the CF, deposition took place in the same direction as the main flow and formed a mouth bar that marks the downflow terminus of the flow (see discussion and figure 17 in Ningthoujam et al., 2022).

METHODS AND TERMINOLOGY

Methods

To better elucidate the stacking pattern of matrix-rich and associated matrix-poor strata, a combination of field-based observations and a statistical analysis was used. Field observations include stratal thickness, bedding contacts, grain size, and sedimentary structures in each bed. Hand samples of matrix-rich and matrix-poor lithologies were collected in the field and then analyzed using an optical petrographic microscope. Individual thin sections were point counted (≥300 points per sample) to accurately describe textural characteristics, and the longest dimension of each framework grain (grain size between 0.0625 mm and 6 mm) was measured to determine grain-size distribution in each sample. Notably, all the petrographic work was conducted by a single operator to minimize operator bias and standardize potential error.

Based on earlier stratigraphic and depositional-framework studies at Castle Creek (WSG), select intervals containing matrix-rich and associated matrix-poor lithologies were chosen for this study. In proximal basin-floor deposits of the Upper Kaza Group, a 100-m-thick and 1000-m-wide stratigraphic interval made up of a succession of terminal splays, distributary channel fill, debrites, thin-bedded turbidites, and matrix-rich and associated matrix-poor strata mapped

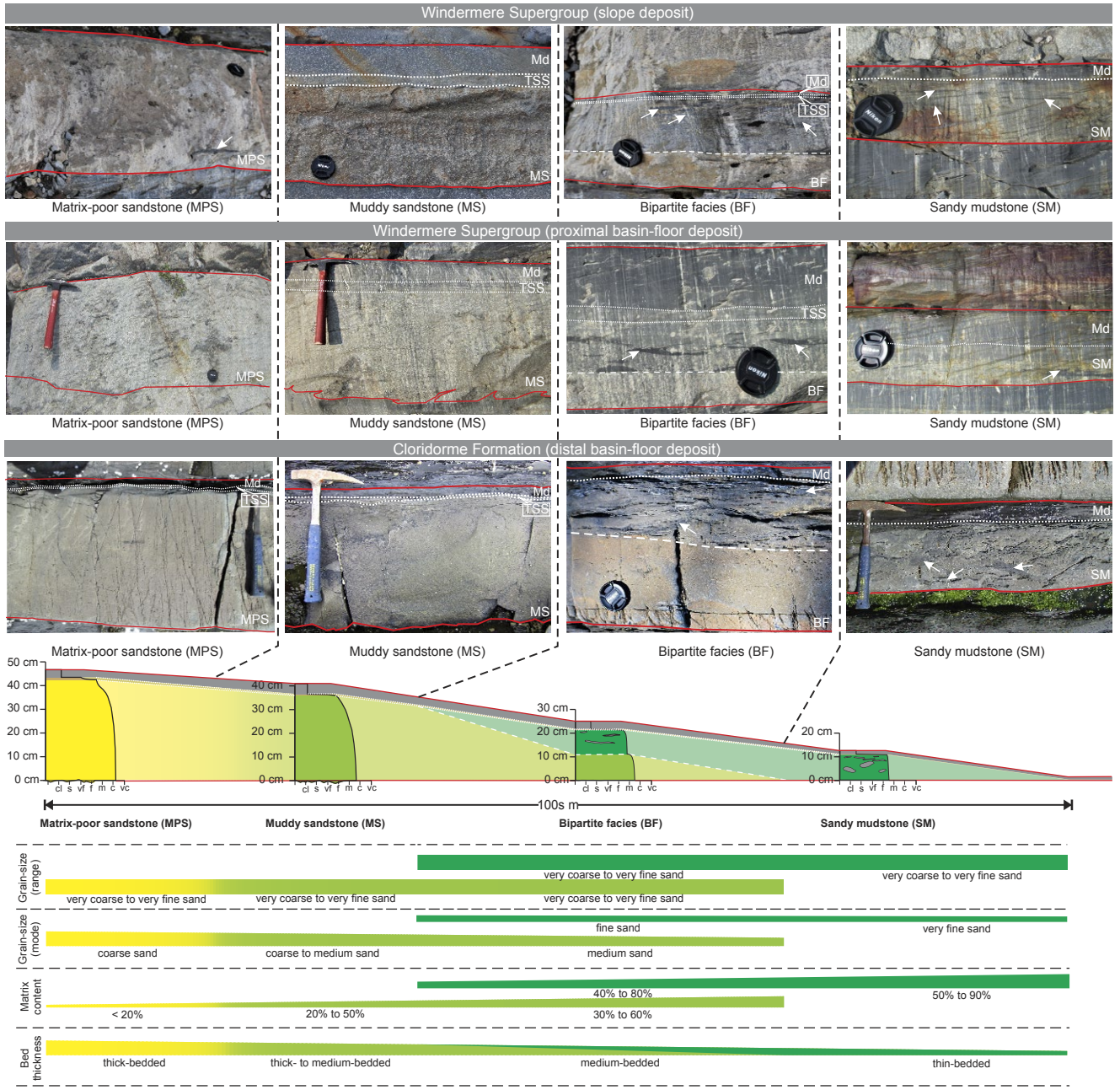

Figure 2. Schematic diagram illustrating idealized proximal to distal (left to right) depositional transect from matrix-poor sandstone (MPS) to muddy sandstone (MS) to bipartite facies (BF) to sandy mudstone (SM) over a distance of hundreds of meters. Except where eroded, the transect is overlain by a thin-bedded traction structured sandstone (TSS) capped by silty mudstone (Md). See Ningthoujam et al. (2022) for descriptive details. Representative photographs of each lithofacies from the Windermere Supergroup and Cloridorme Formation are shown above the transect. Solid red lines mark the base and top of a single bed; white arrows point to mudstone clasts; dashed white lines separate the lower and upper parts of a bipartite facies (BF); dotted white lines mark bases of the traction-structured, very fine-grained sandstone and/or mudstone cap. Scales are: hammer (33 cm long) and camera lens cap (5.2 cm diameter). Bar graphs illustrate general downflow trends in texture (grain-size range, modal grain size, and matrix content) and bed thickness (see Ningthoujam et al., 2022, for details). Grain-size abbreviations: cl—clay, s—silt, vf—very fine sand, f—fine sand, m—medium sand, c—coarse sand, vc—very coarse sand.

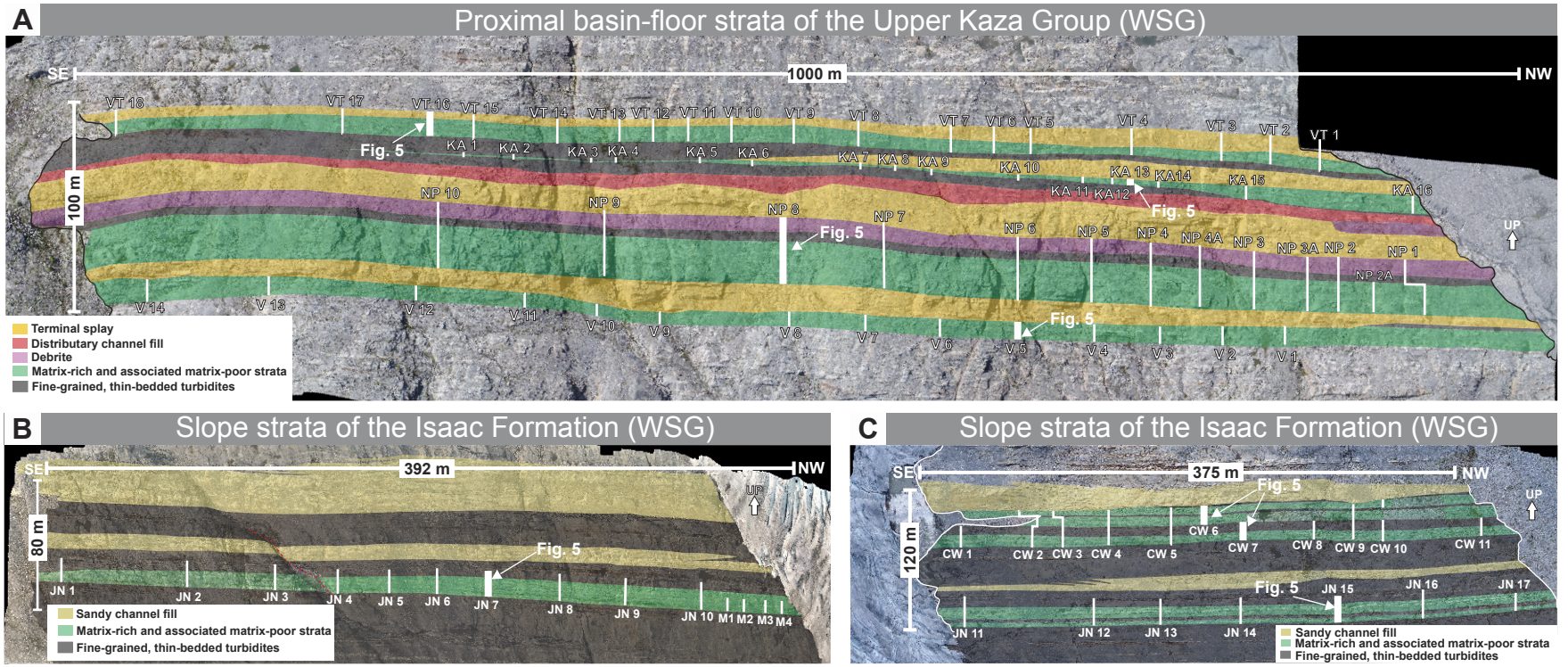

Figure 3. Interpreted drone photographs showing the distribution of stratal elements in proximal basin-floor deposits of the Upper Kaza Group (A) and slope deposits of the Isaac Formation at the Castle Creek study area (B, C). Labeled vertical white lines indicate locations of stratigraphic logs (after Ningthoujam et al., 2022). WSG—Windermere Supergroup.

previously by Terlaky and Arnott (2014, 2016), Terlaky et al. (2016), Angus et al. (2019), and Ningthoujam et al. (2022) was selected. In this section, 61 stratigraphic logs (5–50 m long) were measured over a lateral distance of ~900 m targeting matrix-rich and associated matrix-poor strata (Fig. 3A). Similarly, in slope deposits of the stratigraphically higher Isaac Formation, two stratigraphic intervals (~80 m thick and 400 m wide, and ~120 m thick and 400 m wide) comprising sandy channel fills, thin-bedded turbidites, and matrix-rich and associated matrix-poor strata mapped previously by Arnott (2007a, 2007b), O'Byrne et al. (2007), Angus et al. (2019), Arnott et al. (2021), and Ningthoujam et al. (2022) were selected. Here, a total of 32 logs (3.5–30 m long) were measured in two transects targeting matrix-rich and associated matrix-poor strata (Figs. 3B and 3C). In distal basin-floor deposits of the Petite Vallée member (CF), an ~300-m-thick and 1700-m-wide stratigraphic interval comprising terminal splays, thin-bedded turbidites, and matrix-rich and associated matrix-poor strata mapped previously by Enos (1969), Beeden (1983), Hiscott et al. (1986), and Ningthoujam et al. (2022) was selected. Here, 15 bed-by-bed stratigraphic logs (18–147 m long) were measured (Fig. 4). Also, in both the WSG and the CF, a few logs were extended upward to capture details of the overlying stratal element (Figs. 3 and 4). Additionally, hand samples of matrix-rich and associated matrix-poor lithologies were collected at both study sites, and a total of 253 standard (30 µm thick) thin sections were prepared for conventional petrographic analysis and point counting.

A first-order Markov chain analysis (e.g., Terlaky and Arnott, 2016) was conducted at bed and stratal-unit scales to quantitatively assess how matrix-rich and associated matrix-poor strata stack to build up a stratal element. This statistical technique describes sequential changes in a system composed of discrete, finite states (Krumbein, 1968; Schwarzacher, 1975). The change from one state to the next is considered a transition and is assumed to depend only on the state that precedes it, an assumption termed a first-order Markov property. Also, the system is considered to change randomly

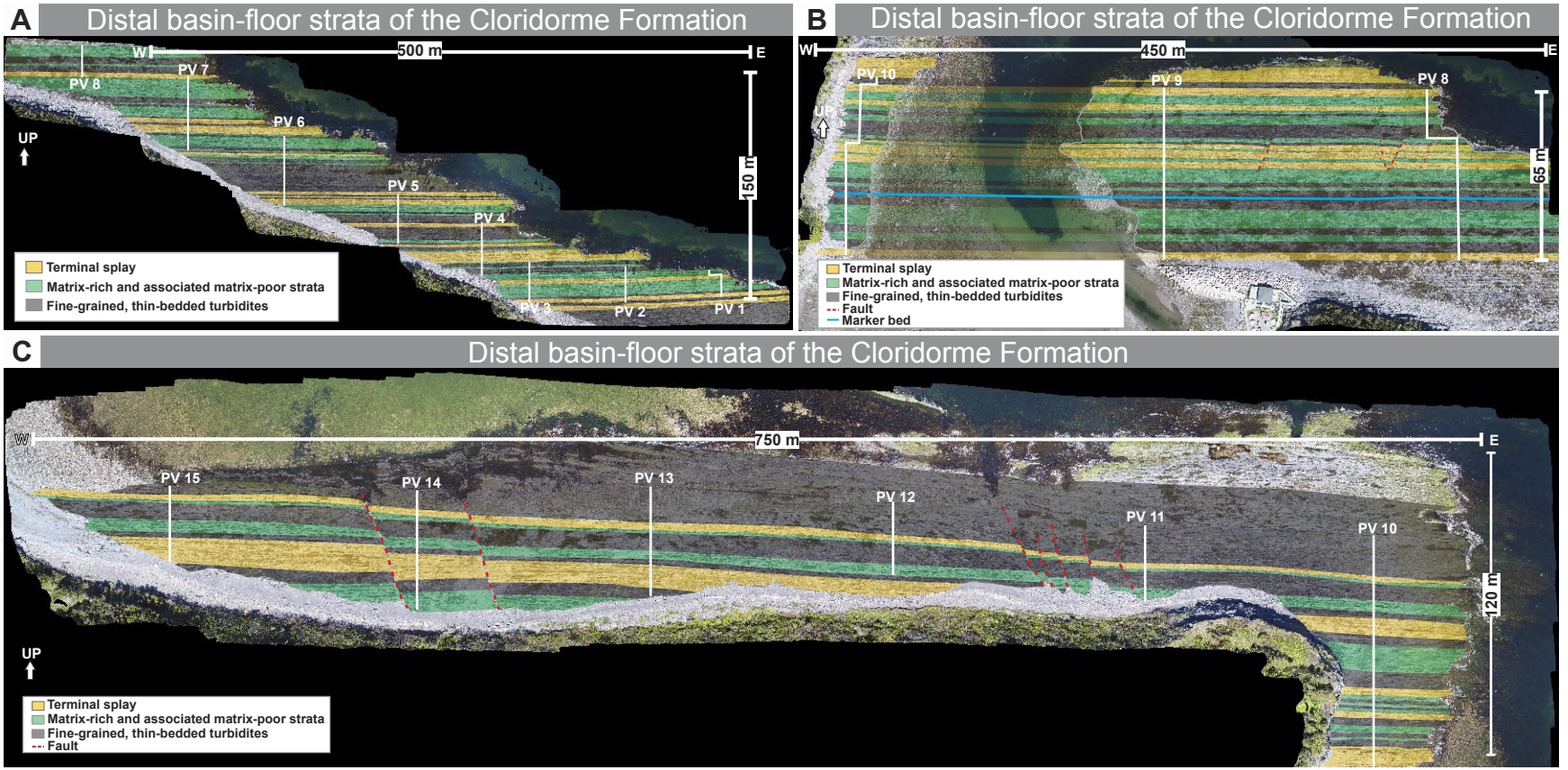

Figure 4. Interpreted drone photographs showing distribution of stratal elements in distal basin-floor deposits of the Petite Vallée study area. Labeled white vertical lines indicate locations of stratigraphic logs (after Ningthoujam et al., 2022).

from one state to another based on the transition probabilities between states. Furthermore, the stratigraphic sections used in this statistical analysis are assumed to be deposited under static paleoenvironmental conditions with no changes due to external forcing (e.g., climate, tectonism, sediment supply) (e.g., Lehrmann and Goldhammer, 1999; Terlaky and Arnott, 2016). Lastly, the vertical transition of states (i.e., from one bed to the next bed, or one stratal unit to the next stratal unit) observed in the stratigraphic sections assumes no erosion and that all states are fully preserved. In the WSG, the input data were obtained from a composite stratigraphic log consisting of all measured matrix-rich and associated matrix-poor strata in the Castle Creek study area. Here, individual logs with the most well-preserved stratigraphy were chosen from each section to build a single continuous 137-m-long stratigraphic section (Fig. 5). In the CF, on the other hand, data were derived from a single, vertically continuous stratigraphic log (286 m long) (Fig. 6). The observed vertical stacking of these strata was then used to construct the transition matrices, which then were tested against the expected transition matrices (zero-order Markov chain, or the null hypothesis) to evaluate statistical significance.

Terminology

In this study, a stratigraphic hierarchy is recognized. At the most basic level, a "bed" consists of one of the four lithofacies recognized by Ningthoujam

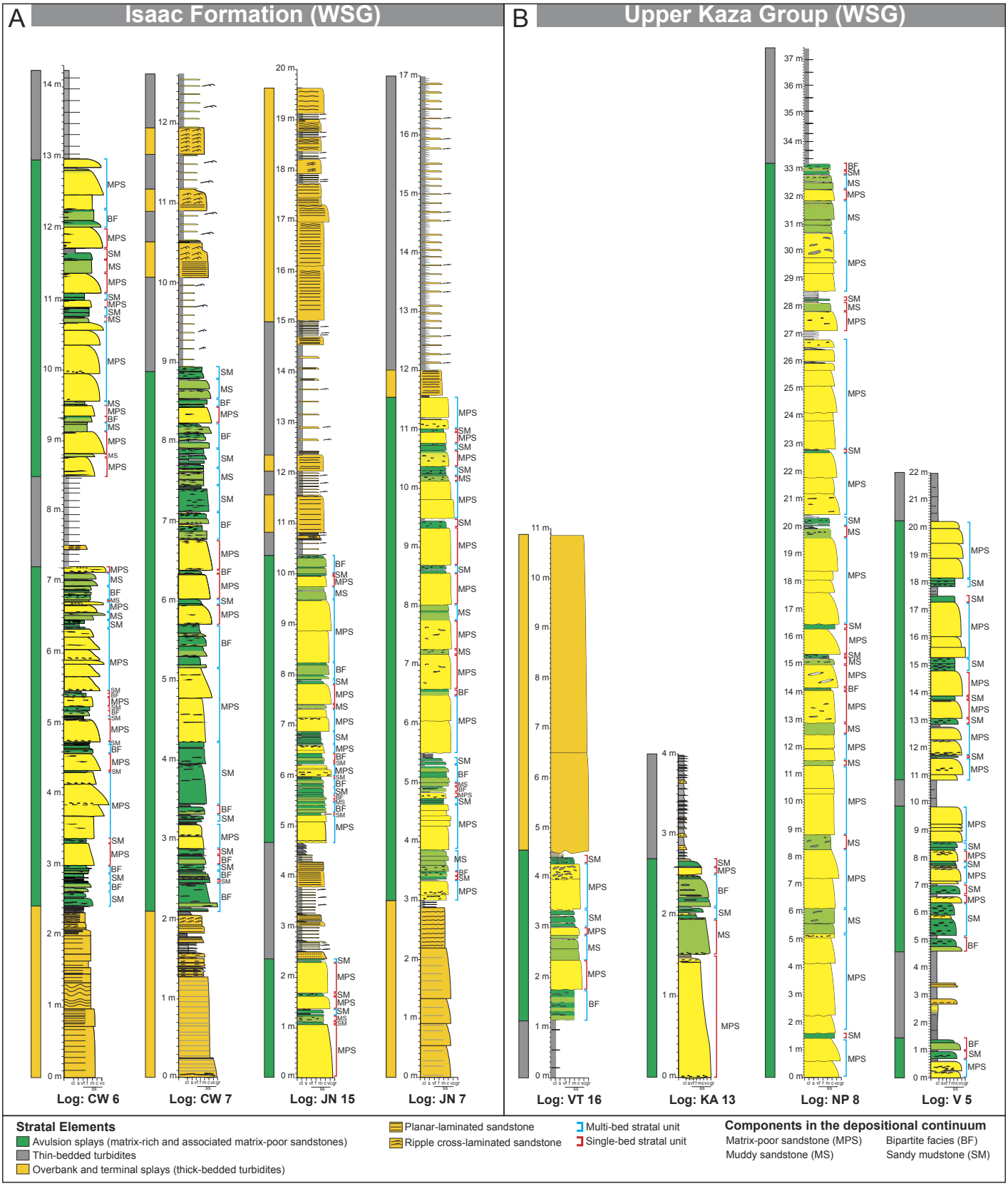

Figure 5. Individual stratigraphic logs used for Markov chain analysis from the Isaac Formation (A) and Upper Kaza Group (B) of the Windermere Supergroup. See Figure 2 for location of individual logs. Matrix-rich and genetically related lithofacies are labeled on the right-hand side of each log. Remaining stratigraphy consists of different types of classical turbidites. Blue brackets indicate beds that are organized into multi-bed stratal units, whereas red brackets, single-bed stratal units. MPS—matrix-poor sandstone; MS—muddy sandstone; BF—bipartite facies; SM—sandy mudstone. Grain-size abbreviations: ss—sandstone, cl—clay, s—silt, vf—very fine sand, f—fine sand, m—medium sand, c—coarse sand, vc—very coarse sand, gr—granule.

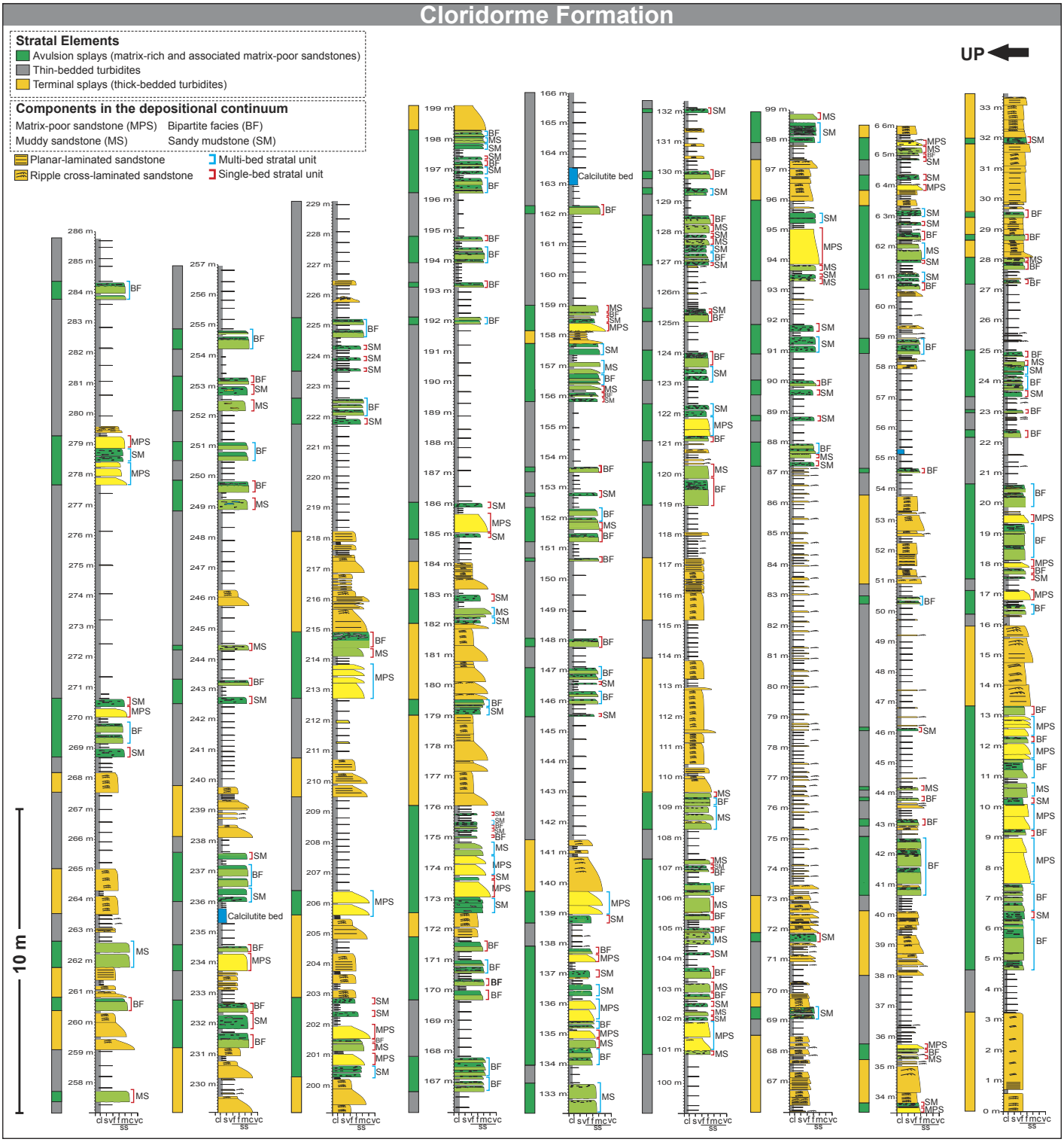

Figure 6. Continuous vertical stratigraphic log in the Petite Vallée study area. Matrix-rich and genetically related lithofacies are labeled on the right-hand side of each log. Remaining stratigraphy consists of different types of classical turbidites. Blue brackets indicate beds that are organized into multi-bed stratal units, whereas red brackets, single-bed stratal units. MPS—matrix-poor sandstone, MS—muddy sandstone, BF—bipartite facies; SM—sandy mudstone. Grain-size abbreviations: ss—sandstone, cl—clay, s—silt, vf—very fine sand, f—fine sand, m—medium sand, c—coarse sand, vc—very coarse sand.

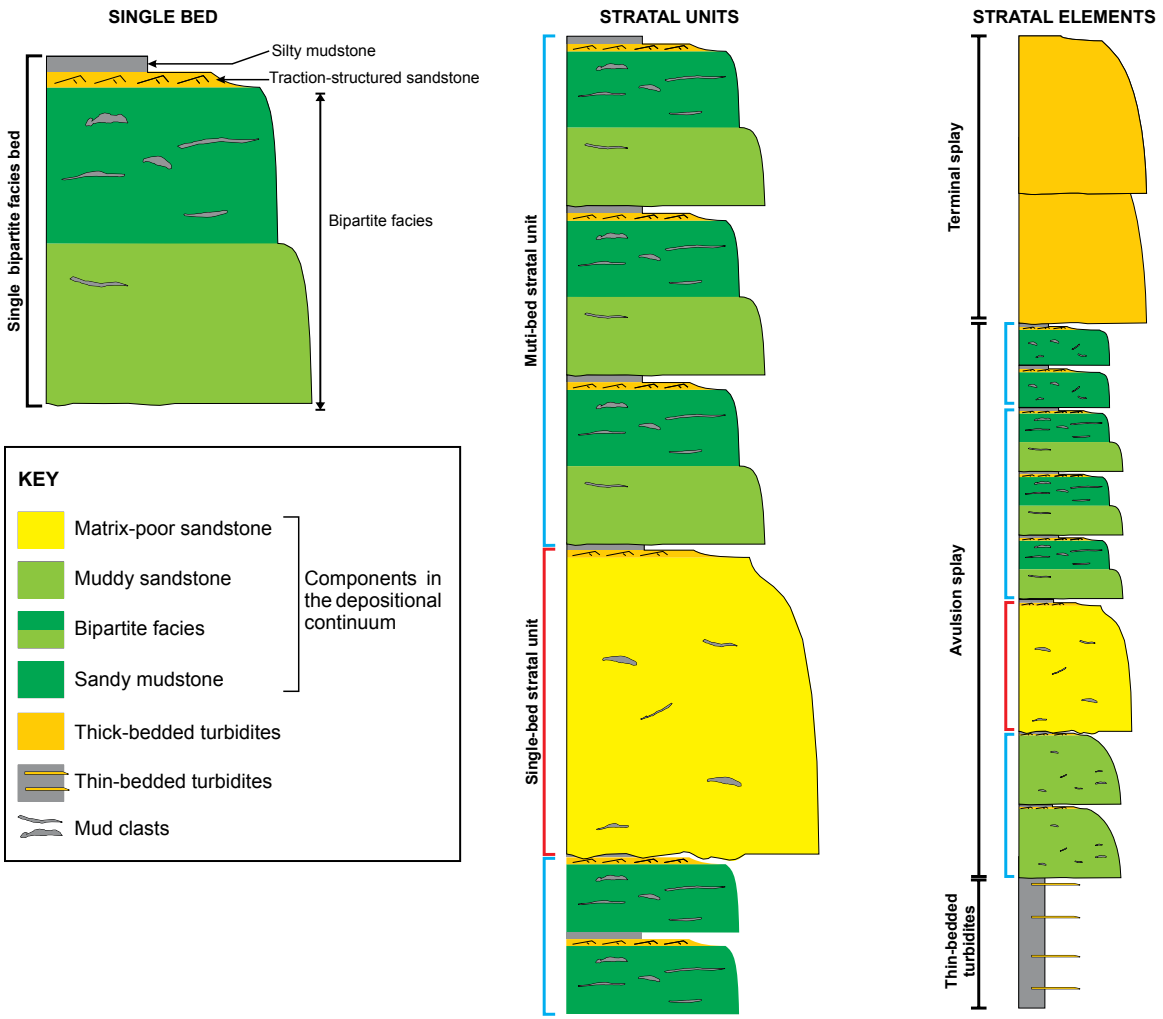

Figure 7. Schematic diagram showing components of a single bed, stratal units, and stratal elements. A single bed (left) or more commonly multiple self-similar beds stack to form a stratal unit (center). Stratal unit boundaries are abrupt and marked by a change to a lithology deposited at a different position along the depositional continuum. Units comprising matrix-rich and associated matrix-poor strata then stack to form a stratal element, here termed an "avulsion splay" (*sensu* Terlaky and Arnott, 2014) (right).

et al. (2022), namely, matrix-poor sandstone (MPS), muddy sandstone (MS), bipartite facies (BF), and sandy mudstone (SM), which, except where eroded, is then capped by a <1-cm- to 10-cm-thick layer of traction-structured sandstone overlain by a silty mudstone. Each bed is then named by the principal lithofacies type (e.g., a bed with BF is called bipartite facies bed) (Fig. 7). Beds then stack to form "units", each of which consists of two or more beds of similar lithofacies type or, less commonly, a single bed that is overlain and underlain by lithologically dissimilar strata (Fig. 7). Additionally, single-bed stratal units occur as single layers intercalated with thin-bedded upper-division turbidites (Fig. 6). Like individual beds, stratal units are named according to the principal lithofacies type (e.g., a stratal unit comprising BF is called a bipartite facies stratal unit). Stratal units then stack to form a stratal "element", which, being composed of either exclusively matrix-rich and associated matrix-poor lithologies or matrix-rich strata intercalated with subordinate thin-bedded turbidite units, is interpreted as an "avulsion splay" (*sensu* Terlaky and Arnott, 2014) (Figs. 5–7).

RESULTS

Stacking Pattern (Bed Scale)

Based on field observations in both study areas, beds of similar lithofacies, but of variable thickness, typically stack (70% of all measured beds in WSG and 65% in CF) to form multi-bed stratal units consisting of two to nine beds (e.g., Figs. 5 and 6). Less commonly (30% of all measured beds in WSG and 35% in CF), the succession consists of single-bed stratal units, which in some places stack but are differentiated from turbidites or other single beds based on unique textural and dimensional attributes (e.g., Figs. 5 and 6). Stratal-unit boundaries are abrupt and typically marked by a change in lithofacies (Figs. 5–7). Beds within a multi-bed stratal unit undergo a transformation from one facies to the next in the lateral depositional continuum, for example, MS to BF, or BF to SM, at about the same lateral position (Fig. 8). Additionally, in the WSG, at any position along a multi-bed stratal unit, the D90 (coarse fraction, 90th percentile of particle size) and D50 (median particle size) of the grain-size distribution subtly and progressively decrease upward (Fig. 9). In the CF, on the other hand, grain-size distribution shows a slight but nonetheless abrupt decrease in the topmost bed in each multi-bed stratal unit (Fig. 10). In both study areas, matrix content changes negligibly upward within a multi-bed stratal unit (e.g., Figs. 9 and 10).

Markov Chain Analysis (Bed Scale)

Descriptive Statistics

A total of 333 and 304 bed transitions were observed in CF and WSG, respectively. Results of the observed and expected transitions of beds in both study areas are summarized in the transition matrix and state diagrams (Fig. 11). In WSG, MPS beds comprise 36% of all beds (i.e., states) observed and are most frequently overlain by similar MPS beds (48% of observed transitions). Less commonly, MPS beds are overlain by beds of SM (27%), MS (20%), or BF (5%). MS beds make up 15% of all the observed beds and most commonly are overlain by other MS beds (34%), and less commonly by beds of SM (28%), MPS (25%), or BF (13%). BF beds constitute 17% of all the beds observed and are most frequently overlain by other BF beds (48%) followed by beds of MPS (25%), SM (21%), or MS (6%). Lastly, SM beds comprise 32% of all the observed beds and are usually overlain by other SM beds (44%), and less commonly by beds of MPS (34%), BF (16%), or MS (6%).

In CF, MPS beds make up 12% of all observed beds and most commonly are overlain by beds of SM (32%) and BF (32%) and less commonly by beds of MPS (29%) or MS (7%). MS beds comprise 16% of all the observed beds and are most frequently overlain by BF beds (48%). Less frequently, MS beds are overlain by other MS beds (25%) and beds of SM (17%) or MPS (10%). BF beds constitute 41% of all observed beds and most commonly are overlain by other BF beds (50%) followed by beds of SM (26%), MS (15%), or MPS (9%). Lastly, SM beds make up 31% of all the observed beds and most frequently are overlain by other SM beds (44%), and less frequently by beds of BF (29%), MS (15%), or MPS (12%).

Significance Test

In the statistical analysis, the degrees of freedom are $(n - 1)^2 = (4 - 1)^2 = 9$, where n is the number of discrete states (i.e., MPS, MS, BF, and SM beds), and the minimum chi-squared (χ^2) value to reject the null hypothesis (at 5% significance level) is 16.92. The values in the χ^2 matrix are calculated using χ^2 = (observed – expected)^2 / expected. The respective sums of the χ^2 matrices are 76 for WSG and 33 for CF (Figs. 11C and 11G). Accordingly, the null hypothesis can be rejected for both study areas and the observed vertical stacking of beds is non-random.

More specifically, comparing the expected and observed transition matrices in both study areas shows that beds of similar lithofacies type typically succeed one another, whereas all other transitions are either less than expected, random, or very close to random (Figs. 11C, 11D, 11G, and 11H). Importantly, in CF, for example, a statistically significant transition does not necessarily correlate with a high or low transition percentage. For example, the transitions from MPS bed to BF bed and MPS bed to SM bed are both 32%, whereas MPS bed to another MPS bed is 29%. Despite the first two transitions being more frequent than the third, the first two are statistically very close to random or random, whereas the third is statistically more likely than random (Fig. 11G). This shows that the most or the least likely transitions in terms of absolute number of occurrences are not necessarily statistically significant and in fact may be only the result of random chance.

Stacking Pattern (Stratal Unit Scale)

In both study areas, stratal units of matrix-rich and associated matrix-poor lithologies stack exclusively to form 0.4–33.2-m-thick (average 2.7 m) avulsion splays (Figs. 5 and 6). These avulsion splays are equivalent in hierarchy to "lobe elements" of Prélat et al. (2009) and in the WSG abruptly underlie sand-rich stratal elements such as slope channels (e.g., Arnott, 2007a, 2007b; Schwarz and Arnott, 2007; Angus et al., 2019; Ningthoujam et al., 2022) (e.g., Fig. 3), distributary channels and terminal splays in the channel-lobe transition zone (Navarro and Arnott, 2020), and proximal basin floor (Terlaky and Arnott, 2014; Terlaky et al., 2016; Angus et al., 2019; Ningthoujam et al., 2022) (e.g., Fig. 3). In distal basin-floor strata of the Petite Vallée study area, the avulsion splays typically underlie terminal splays (see Ningthoujam et al., 2022) (e.g., Fig. 4).

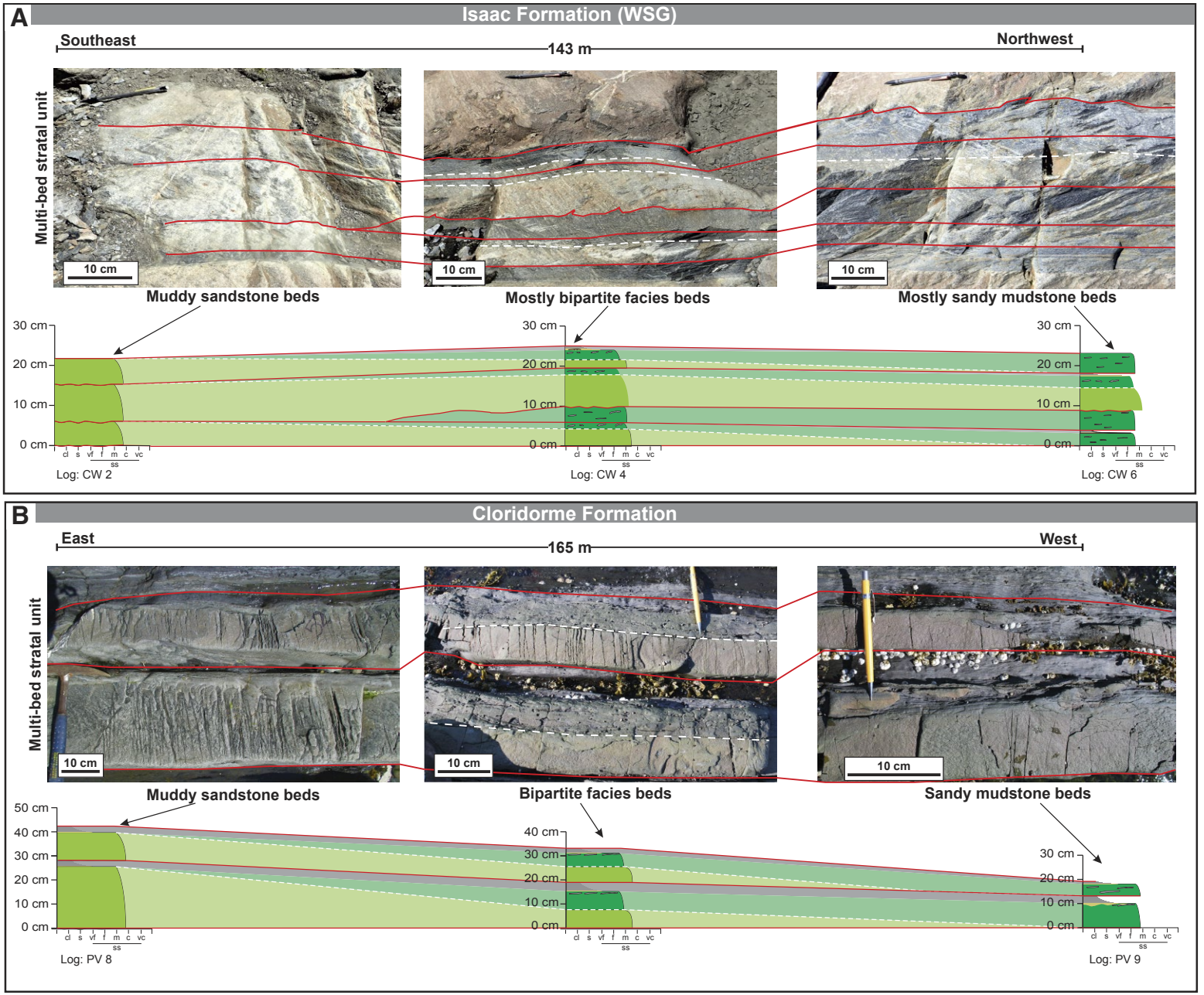

Figure 8. Stratigraphic correlation panel and associated outcrop photographs of a multi-bed stratal element in slope deposits of the Isaac Formation, Windermere Supergroup (WSG) (A) and distal basin-floor deposits of the Petite Vallée member, Cloridorme Formation (B) (see parts 1 and 2 in the Supplemental Material[1] for locations). Note how a stack of lithologically similar beds transitions from more proximal facies (left) to more distal facies (right) at about the same lateral position. Red lines indicate bed contacts, and white dashed lines, the interface in a bipartite facies. Grain-size abbreviations are: ss—sandstone, cl—clay, s—silt, vf—very fine sand, f—fine sand, m—medium sand, c—coarse sand, vc—very coarse sand.

[1]Supplemental Material. Interpreted drone photomosaics and associated correlation panels of stratigraphic sections from the Windermere Supergroup and the Cloridorme Formation showing locations of Figures 8, 9, and 10. Please visit https://doi.org/10.1130/GEOS.S.21913584 to access the supplemental material, and contact editing@geosociety.org with any questions.

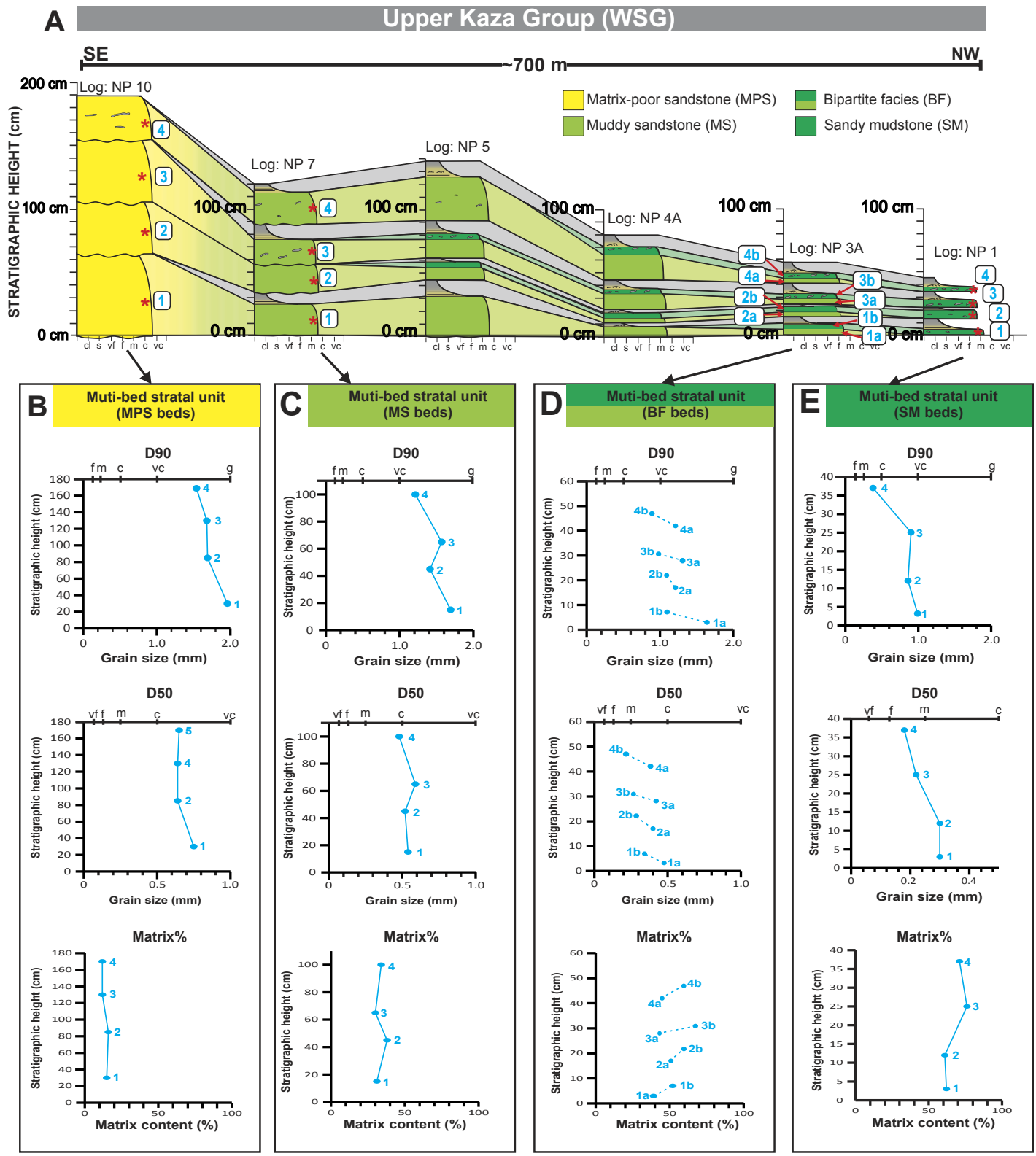

Figure 9. (A) Stratigraphic correlation panel of a multi-bed stratal unit consisting of four individual beds in basin-floor deposits of the Upper Kaza Group, Windermere Supergroup (WSG) (see part 3 in the Supplemental Material [see text footnote 1] for location). Note that in all beds, the transition from matrix-poor sandstone (MPS) to muddy sandstone (MS) to bipartite facies (BF) and sandy mudstone (SM) occurs at about the same lateral position. Samples for microscopic grain-size analysis were collected where one facies transitioned to the next. Sample locations are labeled 1, 2, 3, 4; the "a" and "b" suffixes indicate lower and upper parts, respectively, in a bipartite facies. (B–E) Graphs showing D90 (90th percentile of particle size), D50 (median particle size), and matrix content of a multi-bed stratal unit of MPS, MS, BF, and SM, respectively. Note that at any position along the correlation panel, the matrix content changes little upward, however D90 and D50 subtly but progressively decrease upward. Grain-size abbreviations: cl—clay, s—silt, vf—very fine sand, f—fine sand, m—medium sand, c—coarse sand, vc—very coarse sand.

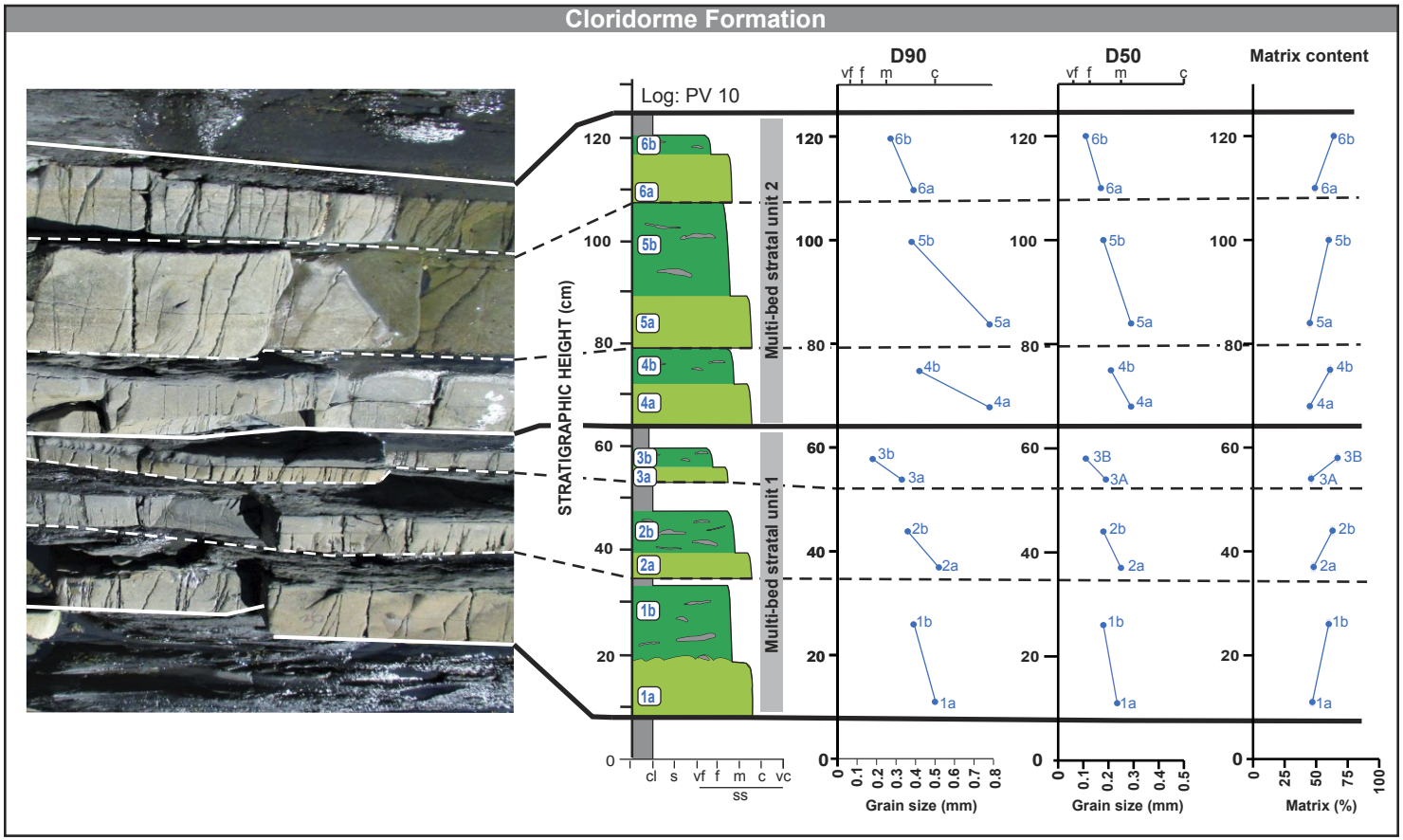

Figure 10. Outcrop photograph and accompanying stratigraphic log of a continuous vertical section showing two multi-bed stratal units consisting of bipartite facies (BF) in the Cloridorme Formation (see part 2 in the Supplemental Material [see text footnote 1] for location). Graphs represent D90 (90th percentile of particle size), D50 (median particle size), and matrix content of the individual beds; "a" and "b" indicate position in lower and upper parts of the bed, respectively. Note that the stratal unit boundary between beds 3 and 4 is based on an abrupt grain-size increase (D90 and D50). Also, note that within each stratal unit, the D90 and D50 show an abrupt decrease in the topmost bed, whereas matrix content changes little. Grain-size abbreviations: ss—sandstone, cl—clay, s—silt, vf—very fine sand, f—fine sand, m—medium sand, c—coarse sand, vc—very coarse sand.

Markov Chain Analysis (Stratal Unit Scale)

Descriptive Statistics

A total of 203 and 184 stratal unit transitions were observed in the CF and WSG, respectively. Results of the observed and expected transitions of stratal units in both study areas are summarized in the transition matrix and state diagrams (Fig. 12). In the WSG, MPS stratal units comprise 34% of all stratal units observed and are most frequently overlain by stratal units of SM (52% of observed transitions). Less commonly, MPS stratal units are overlain by stratal units of MS (30%), BF (14%), or MPS (4%). MS stratal units make up 17% of all observed stratal units and most commonly are overlain by stratal units of SM (50%) and less commonly by MPS (38%) or BF (12%). Furthermore, MS stratal units were not observed to overlie one another. Stratal units of BF constitute 14% of all stratal units observed and are most frequently overlain by stratal units of SM (46%) or MPS (46%), and less commonly by MS (8%). Additionally, BF stratal units were not observed to overlie one another. Lastly, SM stratal units comprise 35% of all observed stratal units and most commonly are overlain by stratal units of MPS (59%) and less commonly by BF (21%), MS (17%), or SM (3%).

In the CF, MPS stratal units make up 12% of all observed stratal units and most commonly are overlain by stratal units of SM (54%) and less commonly by BF (38%) or MS (8%). Additionally, MPS stratal units were not observed to overlie one another. Stratal units of MS comprise 21% of all observed stratal units and are most frequently overlain by BF stratal units (62%). Less frequently, MS stratal units are overlain by stratal units of SM (24%), MPS (7%), or MS (7%).

Markov Chain Analysis (Bed Scale)

Windermere Supergroup (WSG)

A

Observed Transition Matrix - counts (probabilities)

From/To	SM bed	BF bed	MS bed	MPS bed	Total
SM bed	42 (44%)	15 (16%)	6 (6%)	33 (34%)	96
BF bed	11 (21%)	25 (48%)	3 (6%)	13 (25%)	52
MS bed	13 (28%)	6 (13%)	16 (34%)	12 (25%)	47
MPS bed	30 (27%)	5 (5%)	22 (20%)	52 (48%)	109
				Total	304

B

Expected Transition Matrix (for random distribution) - counts

From/To	SM bed	BF bed	MS bed	MPS bed	Total
SM bed	30.3	16.4	14.8	34.4	96
BF bed	16.4	8.9	8.0	18.6	52
MS bed	14.8	8.0	7.3	16.9	47
MPS bed	34.4	18.6	16.9	39.1	109
				Total	304

C

Chi-squared Matrix: $(\text{observed-expected})^2$ / expected

From/To	SM bed	BF bed	MS bed	MPS bed	Total
SM bed	4.5	0.1	5.3	0.1	10
BF bed	1.8	29.2	3.2	1.7	36
MS bed	0.2	0.5	10.5	1.4	13
MPS bed	0.6	10.0	1.6	4.3	17
				Total	76

D

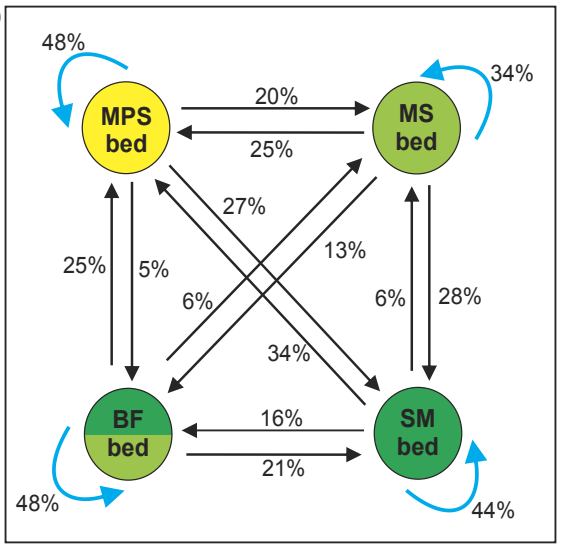

Cloridorme Formation (CF)

E

Observed Transition Matrix - counts (probabilities)

From/To	SM bed	BF bed	MS bed	MPS bed	Total
SM bed	46 (44%)	30 (29%)	16 (15%)	12 (12%)	104
BF bed	36 (26%)	68 (50%)	20 (15%)	12 (9%)	136
MS bed	9 (17%)	25 (48%)	13 (25%)	5 (10%)	52
MPS bed	13 (32%)	13 (32%)	3 (7%)	12 (29%)	41
				Total	333

F

Expected Transition Matrix (for random distribution) - counts

From/To	SM bed	BF bed	MS bed	MPS bed	Total
SM bed	32.5	42.5	16.2	12.8	104
BF bed	42.5	55.5	21.2	16.7	136
MS bed	16.2	21.2	8.1	6.4	52
MPS bed	12.8	16.7	6.4	5.0	41
				Total	333

G

Chi-squared Matrix: $(\text{observed-expected})^2$ / expected

From/To	SM bed	BF bed	MS bed	MPS bed	Total
SM bed	5.6	3.7	0.0	0.1	9
BF bed	1.0	2.8	0.1	1.3	5
MS bed	3.2	0.7	2.9	0.3	7
MPS bed	0.0	0.8	1.8	9.6	12
				Total	33

H

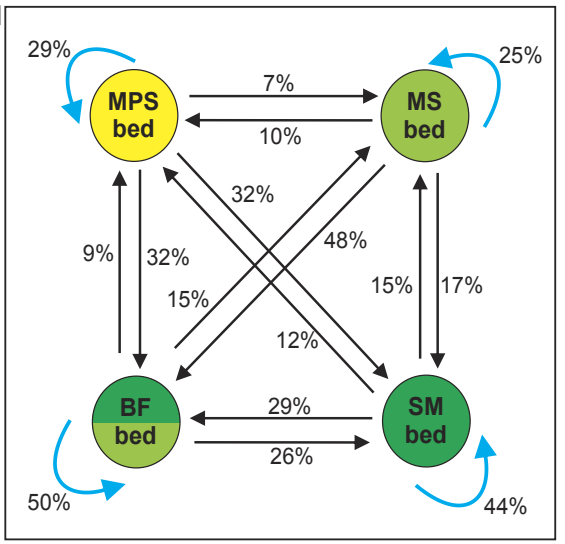

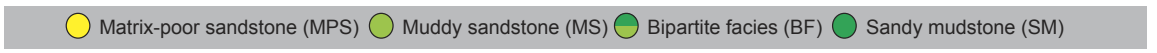

Figure 11. Results of first-order Markov chain analysis of matrix-rich and associated matrix-poor beds in the Windermere Supergroup (WSG; left column) and Cloridorme Formation (CF; right column). Input data are derived from a 137-m-long composite log in the WSG with 304 transitions, and a vertically continuous 286-m-long stratigraphic log in the CF with 333 transitions. MPS—matrix-poor sandstone; MS—muddy sandstone; BF—bipartite facies; SM—sandy mudstone. (A and E) Observed transition matrix counts and probabilities (%). (B and F) Transition matrices showing expected number of transitions in a random system. (C and G) Chi-squared matrices. Blue numbers indicate transitions that are observed more frequently than expected in a random distribution. (D and H) State diagrams showing transition probabilities. Blue arrows indicate transitions observed significantly more frequently than expected based on a random distribution.

Markov Chain Analysis (Stratal Unit Scale)

Windermere Supergroup (WSG)

A

Observed Transition Matrix - counts (probabilities)

From/To	SM (su)	BF (su)	MS (su)	MPS (su)	Total
SM (su)	2 (3%)	13 (21%)	11 (17%)	37 (59%)	63
BF (su)	12 (46%)	0 (0%)	2 (8%)	12 (46%)	26
MS (su)	16 (50%)	4 (12%)	0 (0%)	12 (38%)	32
MPS (su)	33 (52%)	9 (14%)	19 (30%)	2 (4%)	63
				Total	184

B

Expected Transition Matrix (for random distribution) - counts

From/To	SM (su)	BF (su)	MS (su)	MPS (su)	Total
SM (su)	21.6	8.9	11.0	21.6	63
BF (su)	8.9	3.7	4.5	8.9	26
MS (su)	11.0	4.5	5.6	11.0	32
MPS (su)	21.6	8.9	11.0	21.6	63
				Total	184

C

Chi-squared Matrix: $(\text{observed-expected})^2$ / expected

From/To	SM (su)	BF (su)	MS (su)	MPS (su)	Total
SM (su)	**17.8**	1.9	0.0	**11.0**	31
BF (su)	1.1	**3.7**	1.4	1.1	7
MS (su)	2.3	0.1	**5.6**	0.1	8
MPS (su)	**6.1**	0.0	**5.9**	**17.8**	30
				Total	76

D

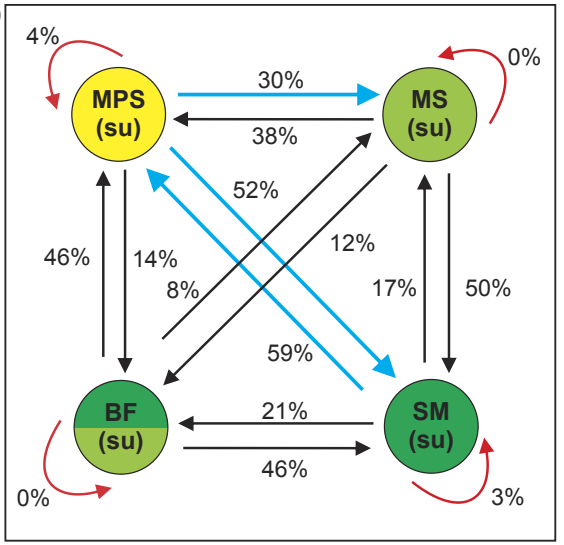

Cloridorme Formation (CF)

E

Observed Transition Matrix - counts (probabilities)

From/To	SM (su)	BF (su)	MS (su)	MPS (su)	Total
SM (su)	7 (11%)	29 (45%)	18 (28%)	10 (16%)	64
BF (su)	34 (47%)	9 (12%)	19 (26%)	11 (15%)	73
MS (su)	10 (24%)	26 (62%)	3 (7%)	3 (7%)	42
MPS (su)	13 (54%)	9 (38%)	2 (8%)	0 (0%)	24
				Total	203

F

Expected Transition Matrix (for random distribution) - counts

From/To	SM (su)	BF (su)	MS (su)	MPS (su)	Total
SM (su)	20.2	23.0	13.2	7.6	64
BF (su)	23.0	26.3	15.1	8.6	73
MS (su)	13.2	15.1	8.7	5.0	42
MPS (su)	7.6	8.6	4.9	2.8	24
				Total	203

G

Chi-squared Matrix: $(\text{observed-expected})^2$ / expected

From/To	SM (su)	BF (su)	MS (su)	MPS (su)	Total
SM (su)	**8.6**	1.6	1.7	0.8	13
BF (su)	**5.2**	**11.3**	1.0	0.7	18
MS (su)	0.8	**7.9**	**3.7**	0.8	13
MPS (su)	**3.9**	0.0	1.8	**2.8**	9
				Total	53

H

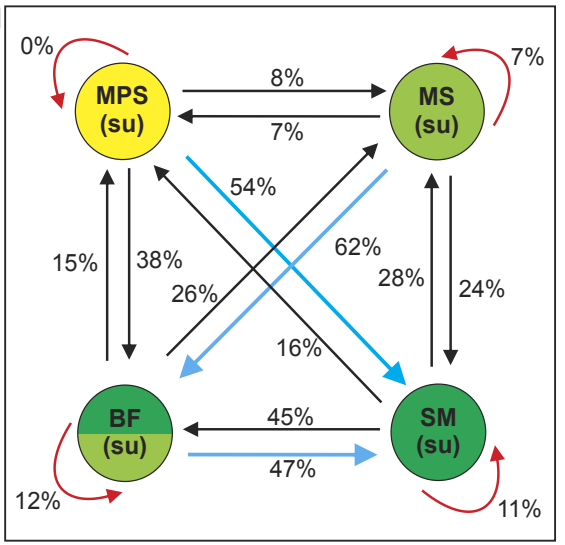

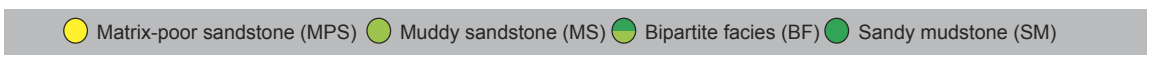

Figure 12. Results of first-order Markov chain analysis of matrix-rich and associated matrix-poor stratal units (su) in the Windermere Supergroup (WSG; left column) and Cloridorme Formation (CF; right column). Input data are derived from a 137-m-long composite log in the WSG with 184 transitions, and a 286-m-long vertically continuous stratigraphic log in the CF with 203 transitions. MPS (su)—matrix-poor sandstone stratal unit; MS (su)—muddy sandstone stratal unit; BF (su)—bipartite facies stratal unit; SM (su)—sandy mudstone stratal unit. (A and E) Observed transition matrix counts and probabilities (%). (B and F) Transition matrices showing expected number of transitions in a random system. (C and G) Chi-squared matrices. Colored numbers indicate the statistically significant transitions: blue numbers indicate transitions that are observed more frequently and red numbers, less frequently than expected in a random distribution. (D and H) State diagrams showing transition probabilities. Statistically significant transitions are colored: blue arrows indicate transitions that are significantly more frequent and red arrows, less frequent than expected in a random distribution.

BF stratal units constitute 36% of all observed stratal units and most commonly are overlain by stratal units of SM (47%) followed by MS (26%), MPS (15%), or BF (12%). Lastly, SM stratal units make up 31% of all the observed stratal units and are most frequently overlain by stratal units of BF (45%) and less frequently by MS (28%), MPS (16%), or SM (11%).

Significance Test

In the statistical analysis, the degrees of freedom are $(n - 1)^2 = (4–1)^2 = 9$, where n is the number of discrete states (i.e., MPS, MS, BF, and SM stratal units) and the minimum chi-squared (χ^2) value to reject the null hypothesis (at 5% significance level) is 16.92. The respective sums of the χ^2 matrices are 76 for WSG and 53 for CF (Figs. 12C and 12G). Therefore, the null hypothesis can be rejected for both study areas and the observed vertical stacking of stratal units is non-random.

Notably, comparison of the expected and observed transition matrices in both study areas shows that similar stratal units are less likely to overlie themselves than expected (Figs. 12C, 12D, 12G, and 12H). With the exception of MPS to MS, MPS to SM, and SM to MPS in the WSG, and MPS to SM, MS to BF, and BF to SM in the CF, all other stratal unit transitions are either random or very close to random (Figs. 12C, 12D, 12G, and 12H).

DISCUSSION

Vertical Stacking (Bed Scale)

Based on field observations and verified statistically, beds of similar lithofacies, but commonly of different thickness, typically succeed one another vertically and form multi-bed (two to nine beds) stratal units; all other transitions are either less than expected, random, or very close to random (Fig. 11). Within a discrete multi-bed stratal unit, successive beds transition from one facies to the next at about the same lateral position (Fig. 8). Also, grain size shows a subtle but nevertheless consistent upward decrease; matrix content changes negligibly upward (Figs. 9 and 10). Collectively, these observations suggest that beds within a multi-bed stratal unit are more or less texturally self-similar and therefore deposited from flows with similar hydraulic and compositional character, albeit exhibiting a minor but nevertheless progressive decrease in flow energy. Superimposed on this temporal regularity is the deposition of the traction-structured turbidite overlain by mudstone that caps each bed. Each cap signals a dramatic change in depositional conditions, which then revert to conditions that resembled those that deposited the underlying bed, albeit commonly with a slightly finer-grained sediment supply. This, then, raises the obvious question as to the origin of such systematic sedimentation and whether deposition of a multi-bed stratal unit is a consequence of multiple flow events or one flow event with multiple pulses.

With respect to multiple flow events, it has been shown experimentally that oversized turbidity currents traversing a partially confined sinuous channel equilibrate to the channel's cross-sectional area by flow stripping and overspill in channel bends, which ultimately reduces size variability in the flows (Straub et al., 2008). More recently, Kelly et al. (2019) described a process termed flow tuning where saline currents passing through a partially confined straight channel adjusted their flow size either by overspilling (oversized flows) or by inflating through ambient fluid entrainment (undersized flows) to achieve an equilibrium flow condition in which overbank losses are balanced with ambient fluid entrainment. Intriguingly, the self-similarity of beds within a multi-bed stratal unit could be consistent with successive flows that had undergone flow tuning; however, variability in the thickness of individual beds within a multi-bed stratal unit (e.g., Figs. 5 and 6) and the subtle but nonetheless consistent upward decrease of grain size observed in multi-bed stratal units makes this problematic (Figs. 9 and 10).

A second possibility is that self-similar beds were deposited from multiple pulses of a single turbidity current. Pulsing in turbidity currents has been recognized in direct monitoring of natural flows (e.g., Shepard et al., 1975; Best et al., 2005; Menczel and Kostaschuk, 2013) and studied experimentally and simulated numerically (e.g., Dai, 2008; Ho et al., 2018a, 2018b; Kostaschuk et al., 2018); however, relatively few studies have described evidence of this in the ancient sedimentary record. In Lowe (1982) and Larue and Provine (1988), stacks of self-similar turbidites lacking evidence of intervening erosion were suggested to have been formed by pulsations or surges in velocity during a single flow event. Additionally, alternating arenite and pelite turbidite facies, equivalent to stacked Bouma Tcd/e (upper division turbidite beds) divisions, were reported from Oligocene and Carboniferous rocks in eastern France by Duringer et al. (1991) and interpreted to have been deposited by a single, continuous muddy turbidity current with episodic higher-energy pulses forming the Tc divisions. Also, in the Precambrian Kongsfjord Formation in Norway, Pickering (1979) interpreted ~2–5-m-thick bedsets, each comprising at least five beds and composed mostly of upper-division turbidites and exhibiting a progressive upward fining and thinning, to record pulses of traction-transport deposition separated by lower-energy suspension deposition during a single continuously waning flow event. Most recently, Cunningham and Arnott (2021) described thin-bedded, upper-division turbidites in continental-slope levee deposits in the WSG that form bedsets of about two to ten self-similar beds, which they attributed to deposition from multiple episodic pulses of a single channelized flow event.

Although it seems clear from these outcrop examples that stacked bed self-similarity is suggestive of turbidity current pulsing, the cause for the pulsing still remains poorly understood. To date, a variety of mechanisms have been proposed to explain pulsing, including: high swell waves and high tides generating pulsating turbidity currents (Shepard et al., 1975); retrogressive slumping that evolved downslope into multi-pulsed turbidity currents (Piper et al., 1999; Canals et al., 2004; Ho et al., 2018a); multi-pulsed flows formed downflow of channel confluences by discrete flows triggered simultaneously (e.g., by an

earthquake) in different upflow channels such as tributaries in a canyon system (Nakajima and Kanai, 2000; Ho et al., 2018a); velocity pulsing caused by hydrodynamic instabilities in plunging hyperpycnal flows (Kostaschuk et al., 2018); hypo- and mesopycnal flows generating multiple secondary turbidity currents through settling-driven Rayleigh-Taylor convection (Hoyal et al., 1999; Parsons et al., 2001; Davarpanah Jazi and Wells, 2016, 2020). Additionally, in some confined settings, like in the CF, flow reflection has been suggested to cause pulsing in turbidity currents (e.g., Haughton, 1994; Ho et al., 2018a). Most of these mechanisms, except for retrogressive slope failures, are expected to have short delay times (few minutes to hours) between pulses, which would preclude the emplacement of the traction-structured sandstone and mud cap over individual beds in a bedset. In a multi-pulsed flow initiated by retrogressive slumping, the time between successive slope failures can be sufficient to allow for the deposition and preservation of traction-structured sandstone and mud cap, but it is highly unlikely to result in consistent self-similarity of successive pulses of sediment transport and deposition. Additionally, the subtle but nevertheless consistent upward-fining trend observed in all multi-bed stratal units is difficult to reconcile with any of these mechanisms (Figs. 9 and 10).

An alternative mechanism builds on recent direct monitoring of turbidity currents in the Congo Canyon by Azpiroz-Zabala et al. (2017). Unlike typical laboratory-generated surge-type turbidity currents, where the body is faster than the head and continuously feeds the head with sediment (e.g., Middleton, 1966), Azpiroz-Zabala et al. reported that Congo Canyon turbidity currents consist of a dense, fast-moving and erosive head, termed a "frontal cell", and a trailing body and tail (Fig. 13A). Here, the flow is sustained by the frontal cell through continuous erosion and incorporation of new sediment from the seafloor while simultaneously shedding sediment-laden fluid into the trailing part of the flow. The difference in density and hence velocity between the frontal cell and the rest of the flow (i.e., the body and tail) allows the frontal cell to outrun the trailing flow and stretch the flow downstream. This process also allows turbidity currents to last as long as 10 days compared to a few minutes to hours in previous flow measurements in other modern systems (e.g., Xu

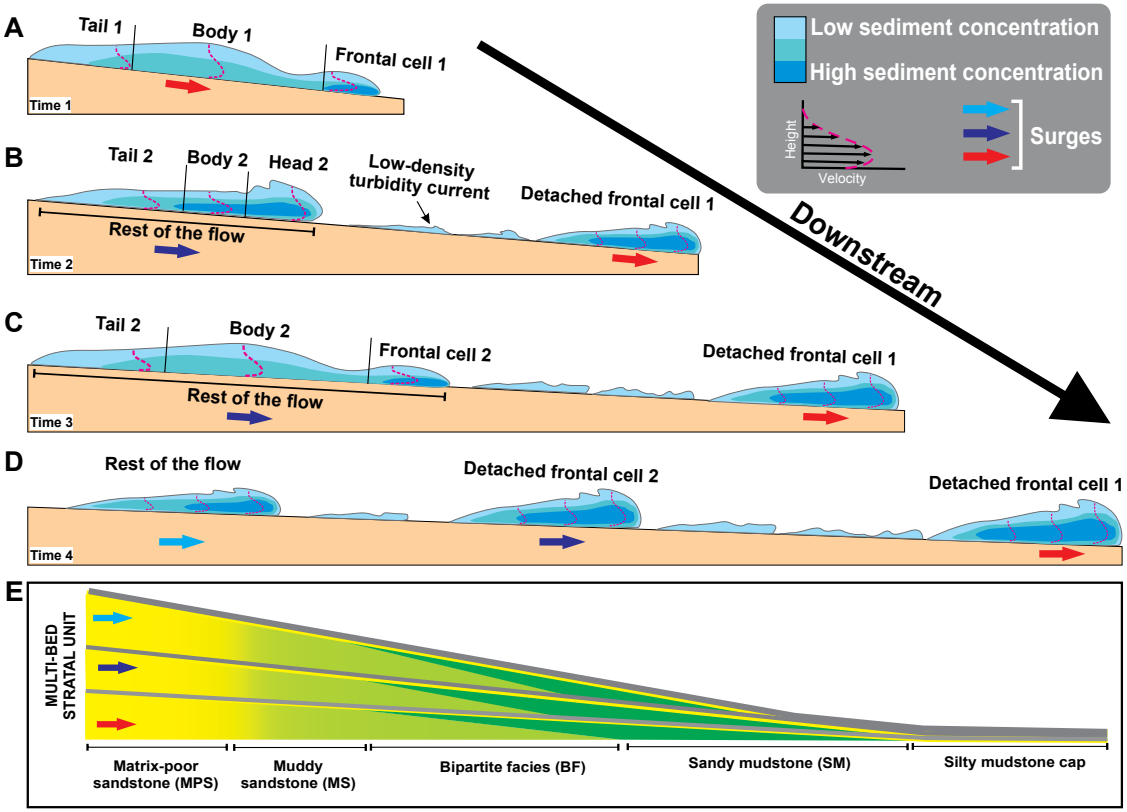

Figure 13. Schematic diagram illustrating development of multiple surges from a single turbidity current. Figures are not to scale. (A) Turbidity current consists of a dense, fast-moving erosive head (frontal cell) and a trailing body and tail. (B) Frontal cell detaches from the rest of the flow and becomes a separate turbidity current. (C) Increased density in the new head causes it to accelerate, possibly eroding the seafloor, and form a new frontal cell (frontal cell 2). (D) Frontal cell 2 then detaches from the rest of the flow and becomes a discrete turbidity current. With time and distance downslope, this process is possibly repeated several times, creating multiple surges from a single flow event. (E) Successive surges deposit a stack of self-similar beds that build up a multi-bed stratal unit. Importantly, the time lag between surges is sufficient to allow for deposition of the traction-structured sandstone and/or mudstone cap.

et al., 2004; Khripounoff et al., 2012; Liu et al., 2012; Hughes Clarke, 2016). Considering that the flow monitoring by Azpiroz-Zabala et al. was limited to the submarine canyon and that at least some turbidity currents are capable of reaching further downslope and even onto the basin floor, it is possible that as the turbidity current continues to be stretched, the dense frontal cell eventually becomes detached from the rest of the flow and forms a separate turbidity current (Fig. 13B). With the detachment of the head, the remaining (main) turbidity current is cut off from its major source of sediment, which then causes it to be diluted and slow. Additionally, elevated stagnation pressure at the new leading edge of the main flow causes it to move more slowly than the trailing part, which then feeds sediment forward and into a newly developing head (Middleton, 1966; Kneller and Buckee, 2000; Cartigny et al., 2013). With time, increased density in the head causes it to accelerate and erode the seafloor, which then feeds new sediment into the head and also sheds into the trailing body. Farther downflow, the head evolves into a new frontal cell (Fig. 13C) that eventually detaches from the main flow and becomes a second discrete turbidity current (Fig. 13D). With time and distance downslope, this process is possibly repeated several times, creating multiple surges from a single flow event. Accordingly, each bed in a multi-bed stratal unit would correlate with a single surge (Fig. 13E), and the progressive decrease in grain size reflects the gradual long-term waning of the parent turbidity current. Additionally, single-bed stratal units that separate multi-bed stratal units or occur as a single layer in a succession of thin-bedded turbidite units (Figs. 5 and 6) may indicate flows where only the initial surge (i.e., first detached head) reached that downslope position while the rest of flow terminated some distance further upslope.

Importantly, the delay time between successive surges must have been sufficient to allow for the emplacement of traction-structured, very fine-grained sandstone (0.2–3 cm thick) and overlying mud cap. Similar low-frequency pulses have also been suggested by Cunningham and Arnott (2021) to allow for the deposition and semi-consolidation of silty and muddy Td/e divisions overlying self-similar sand-rich Tc divisions in continental-slope levee deposits of the Isaac Formation (WSG). Potentially more significant is the mud cap, which typically is massive and 3–5 cm thick. Here the rapid accumulation of fine-grained sediment is attributed to very high near-bed sediment concentration and extensive particle-particle interaction that promoted mud flocculation and aggregation (McAnally et al., 2007; see also discussion in Cunningham and Arnott, 2021). Particle aggregation may also have been enhanced by mud particle adhesion to suspended microbial extra-cellular polymeric substances (EPS) (Bennett et al., 1992). Given the absence of bioturbation in WSG and CF strata, it is possible that the mud-rich seabed was anomalously enriched in microbes and associated EPS, which, when eroded during avulsion, resulted in rapid and extensive particle aggregation in the near-bed region. Eventually, the concentration of flocculated and aggregated particles led to gelling and *en masse* deposition of the mud layer. Notably, the contact between a mud cap and the overlying bed in a multi-bed stratal unit is typically sharp and planar. This indicates that the mud caps had sufficient strength and load-bearing capacity to resist shearing and loading during deposition of the overlying bed. If strength were to have developed through self-weight consolidation (i.e., normal consolidation; Skempton, 1969), the time frame would have greatly exceeded the predicted delay time between surges associated with a single flow event. However, based on observations of modern deep-marine sediments in offshore Angola and Nigeria, the Nova Scotian Slope, and in the Pacific Ocean (Baltzer et al., 1994; Meadows and Meadows, 1994; Ehlers et al., 2005; Kuo and Bolton, 2013), a zone of exceptionally high strength, albeit with high water content, and termed the "crust" (*sensu* Kuo and Bolton, 2008) occurs a few tens of centimeters to about a meter below the seafloor with strength that is an order of magnitude higher than from normal consolidation. Although development of the crust is still poorly understood, microbially mediated strength enhancement of marine sediments through production of EPS has been proposed in several studies (e.g., Dade et al., 1990; Tolhurst et al., 2002; Bhaskar and Bhosle, 2005). Additionally, Parkes et al. (2000) showed that the concentration of bacteria in the uppermost meter of the marine sediment pile can exceed 10^9 cells per cubic centimeter of sediment and rival that in the terrestrial realm. Using similar concentration of microbes (i.e., 10^9 cells per cubic centimeter of sediment) as measured in modern subsurface marine sediments, Dade et al. (1996) experimentally showed that a glue-like exopolymer produced by marine bacteria (*Alteromonas atlantica*) enhanced the yield stress of a kaolinite clay and seawater mixture by 60% in ~0.5–9 days. Collectively, it is postulated that a lag of possibly several days between successive surges, combined with biophysically enhanced mud particle aggregation in the near-bed region, led to gelling, and *en masse* deposition of the mud layer, as well as microbe-induced post-depositional strength enhancement of the mud layer, allowed for the deposition and preservation of mud caps associated with successive surges during the same flow event.

Vertical Stacking (Stratal Unit Scale)

Results of the Markov chain analysis of matrix-rich and associated matrix-poor lithologies at the stratal unit scale show that similar lithologies that make up part of the depositional continuum in each of their respective stratal units stack less commonly than expected in a random distribution in both study areas, whereas stratal unit transitions of MPS to SM, SM to MPS, and MPS to MS in the WSG and MS to BF, BF to SM, and MPS to SM in the CF are observed significantly more frequently than expected in a random distribution (Figs. 12C, 12D, 12G, and 12H). This indicates that the observed vertical stacking in both study areas is more heterogeneous than predicted by a random distribution of stratal units, and the fact that this statistical analysis (see Methods and Terminology section above) assumes no external forcing (e.g., variations in sediment supply, changes in relative sea level, tectonic variability) but also the commonality of these distinctive strata in the deep-water stratigraphy of both the WSG and CF imply an internal forcing.

In WSG strata, the stack of the thickest and most proximal lithofacies in a single stratal unit (i.e., MPS stratal unit) is preferentially overlain by a stack of

the thinnest and most distal lithofacies in the overlying stratal unit (i.e., SM stratal unit), or vice versa (Figs. 12C and 12D). Considering that these strata were deposited on opposite ends of the depositional continuum, the stacking pattern indicates an abrupt and long-distance lateral displacement of facies. This is the stratigraphic manifestation of compensational stacking, which here resulted from the flows being diverted around topographic highs formed by deposition of the previous stratal unit and directed into adjacent topographic lows (Terlaky and Arnott, 2016) (Fig. 14A). Flow diversion was followed by a temporary stabilization of flow and sedimentation conditions and deposition of the next stratal unit. MPS stratal units are also preferentially overlain by slightly more distal MS stratal units, however the opposite transition (i.e., MS to MPS) is shown not to be statistically significant (χ^2 value of 0.1) (Figs. 12C and 12D). The MPS-overlain-by-MS transition indicates a minor back-step of successive stratal units that might reflect flow deceleration against the positive relief created by deposition of the underlying stratal unit (Pratson et al., 2000; Ferguson et al., 2020) (Fig. 14A). In the CF strata, on the other hand, preferential stacking of stratal units including MS to BF, BF to SM, and MPS to SM are observed (Figs. 12G and 12H). Notably, however, the inverse of these transitions shows no statistical significance, suggesting a strong preference for systematic back-stepping at the stratal unit scale. As noted earlier, matrix-rich and associated matrix-poor strata in the CF form mouth-bar deposits at the downflow terminus of the flow (see Ningthoujam et al., 2022); therefore, this systematic back-stepping of stratal units most likely represents accretion on the upflow side of the mouth bar (Fig. 14B).

Overall, results of the statistical analysis suggest a preferred growth pattern of stratal units consisting of initiation followed by gradual back-stepping and then side-stepping into an adjacent topographic low (WSG) or consistent back-stepping (CF). The stacking pattern can either occur once or repeat multiple times building up several-meters-thick stratal elements termed avulsion splays (Terlaky and Arnott, 2014). A similar growth pattern is commonly reported from submarine fans and at a variety of scales, including beds and/or bedsets (e.g., Deptuck et al., 2008; Jobe et al., 2017), lobe elements (e.g., Deptuck et al., 2008; Jegou et al., 2008), and lobes (e.g., Twichell et al., 1991; Vittori et al., 2000; Fildani et al., 2018). The cause for this systematic growth pattern

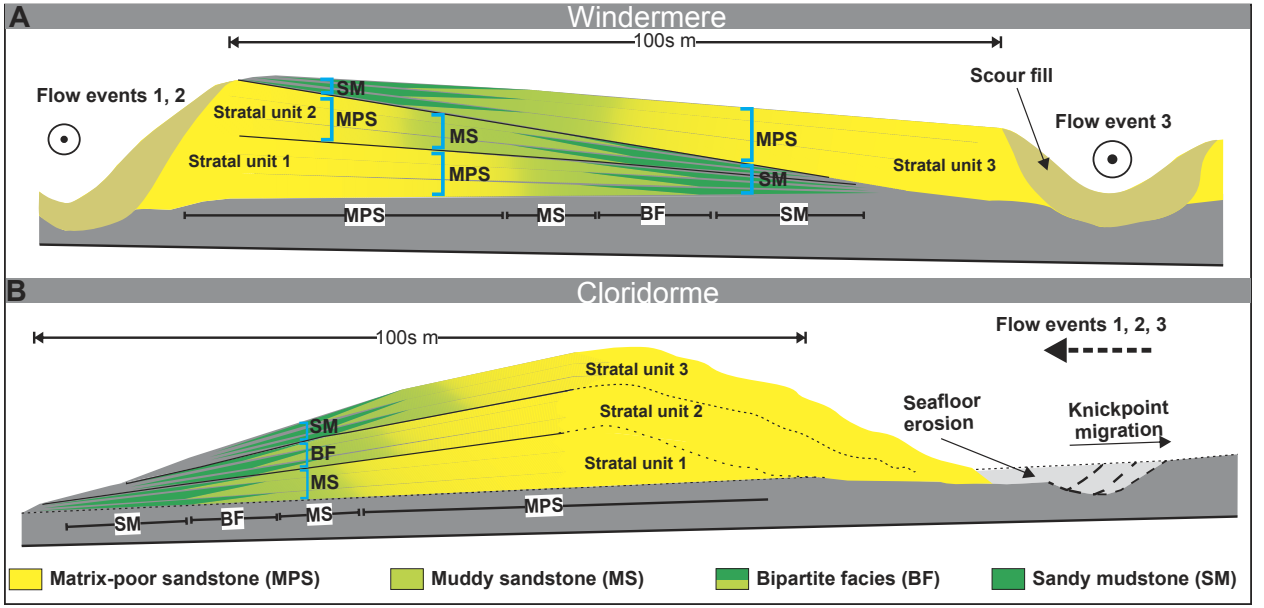

Figure 14. Schematic diagrams illustrating statistically preferred stacking patterns of matrix-rich and associated matrix-poor stratal units in the Windermere Supergroup (WSG) (A) and Cloridorme Formation (CF) (B). Figures are not to scale. In A, local flow is into or out of the page, whereas flow is from right to left in B. MPS—matrix-poor sandstone stratal unit; MS—muddy sandstone stratal unit; BF—bipartite facies stratal unit; SM—sandy mudstone stratal unit. Stratal units 1, 2, and 3 collectively build up an avulsion splay. Each stratal unit, consisting of one or more beds, correlates to a single flow event. (A) In the WSG, note minor back-stepping of stratal units 1–2 that is manifest by the vertical transition of MPS to MS. This is then followed by a significant side-stepping of stratal unit 3 marked by MPS overlain by SM and vice versa—a stacking pattern better known as compensational stacking. (B) In the CF, note the preference for stratal unit back-stepping, which is expressed by systematic stacking of MS to BF to SM.

is still a topic of debate, and studies have associated it with either allogenic controls, like sea level and climate (Hodgson et al., 2006; Marsset et al., 2009; Romans et al., 2009; Jobe et al., 2017), or internal autogenic controls, like the interaction between flows and the evolving topography (Gervais et al., 2006; Jegou et al., 2008; Prélat et al., 2009). Although allogenic forcing may exert some influence on the depositional pattern of the packages described here, Cantelli et al. (2011) and Fernandez et al. (2014) showed experimentally that similar depositional patterns (i.e., forward-stepping, back-stepping, and then side-stepping of the depocenter) can be generated with no change in allogenic conditions. Additionally, more recent numerical modeling (Burgess et al., 2019) and physical experiments (Ferguson et al., 2020) showed that in unconfined settings like the basin floor, even when external factors change, being sediment supply in these studies, the effect of depositional topography (i.e., autogenic forcing) on the evolution and orientation of the flows dominated and generated depositional patterns that were largely similar to those in earlier studies with constant sediment supply.

Even though results of the statistical analysis show that the stacking pattern of lithofacies stratal units making up an avulsion splay are similar to many of the bed-and/or bedset- to lobe-scale stacking patterns recognized in both modern and ancient deep-marine systems, the composite strata are unique in their high mud content, which then requires an abrupt and temporarily sustained supply of mud. As interpreted above, and previously by Terlaky and Arnott (2014), Angus et al. (2019), and Ningthoujam et al. (2022), the abrupt development of matrix-rich strata is caused by an upflow avulsion that activates the local transport system. During avulsion, the flow loses confinement and forms a wall jet that locally scours the muddy inter-channel area, thereby charging the flow with mud (see Ningthoujam et al., 2022). The scour locally steepens the seafloor gradient, forming an upflow-migrating knickpoint that locally increases the erosive potential of successive flows (e.g., Fildani et al., 2013; Carvajal et al., 2017). Upflow-migrating knickpoints have become increasingly recognized in studies of the modern seafloor and shallow subsurface, especially those using high-resolution seafloor imaging techniques (e.g., Fildani et al., 2006, 2013; Armitage et al., 2012; Carvajal et al., 2017; Maier et al., 2020). Described as either "train of scours" or "erosional steps" (e.g., Fildani et al., 2006, 2013), these features have been related to the upstream migration of cyclic steps sculpted by turbidity currents, which in essence are a train of spaced hydraulic jumps that in modern systems have been shown to occur where sediment gravity flows lose confinement, like in the overbank area of an adjacent active channel (e.g., Fildani et al., 2006; Armitage et al., 2012) and downflow of a break in slope (Carvajal et al., 2017; Maier et al., 2020). Here, regardless of the process that causes the avulsion or where it occurs, it is postulated that erosional knickpoint retreat not only charged the flows with fine-grained sediment, but in conjunction with the depositional bulge created by the underlying stratal unit, drove the systematic back-stepping of successive stratal units (e.g., Fig. 14B) (see also Carvajal et al., 2017). Moreover, in the case of the CF example, the knickpoint scour is not part of a train of scours but instead a solitary feature at the terminus of the channel, and like in the WSG, depositional conditions were controlled by changes in effective fluid viscosity caused by the incorporation of eroded mud rather than changes in hydraulic flow conditions and/or transformations in flow type (Ningthoujam et al., 2022).

A similar history of knickpoint formation and headward migration associated with local submarine channel avulsion has been interpreted from seismic images in the Late Pleistocene Amazon and Rhône submarine fans by Pirmez et al. (2000). Downflow of the avulsion node, these authors noted a lobate, high-amplitude (i.e., sand-rich), sheetlike deposit they termed a "high-amplitude reflection packet" (HARP), which here, like in Terlaky and Arnott (2014), is termed an avulsion splay. As stratal units accumulate, local topography increases and eventually causes flows to be diverted into adjacent topographic lows, such as the thin, fine-grained fringes of the depositional continuum. With these diverted flows experiencing an abrupt gradient change, a new knickpoint is created (see also Pirmez et al., 1997), and the process repeats with the deposition of the next stratal unit of matrix-rich lithologies. This combination of knickpoint migration and local topographical steering continues to form matrix-rich deposits until the supply of mud from local seafloor erosion becomes exhausted, quite possibly due to scour down to a sufficiently compacted subsurface layer, the avulsion node healing, the muddy substrate becoming buried in sand, or the parent channel diverting to a new location.

CONCLUSIONS

Matrix-rich and associated matrix-poor sandstones typically underlie sand-rich stratal elements like slope channel, distributary channel, and terminal splay deposits in the Windermere Supergroup (WSG) and terminal splays in the Cloridorme Formation (CF). This association is interpreted to be related to the activation of the local transport system caused by an upflow avulsion. Avulsion formed a wall jet that locally scoured the mud-rich inter-channel area and charged the flow with fine-grained sediment, namely very fine sand to clay, in addition to low-density mud clasts. The local incorporation of easily suspended fine-grained sediment resulted in an abrupt increase in local effective viscosity and a dramatic change in the characteristics and reduction in the diffusion of turbulence required to maintain the particle suspension. This caused the sediment suspension to rapidly exceed transport capacity and collapse, forming a negligibly sheared suspension that deposited a systematic along-flow depositional continuum consisting of matrix-poor sandstone (MPS) to muddy sandstone (MS) to bipartite facies (BF) and then sandy mudstone (SM) over a distance of hundreds of meters and collectively overlain by a thin-bedded, traction-structured sandstone and/or silty mudstone cap. Deposition of this transect occurred along the margins of the high-energy wall jet in the WSG, but at the downflow terminus of the flow in the CF.

Vertically, and at the bed scale, similar lithofacies tend to preferentially stack and build up multi-bed stratal units two to nine beds thick. The grain-size distribution within a multi-bed stratal unit shows a subtle but nevertheless consistent upward-fining trend, whereas the matrix content changes little

upward. Additionally, within a discrete multi-bed stratal unit, individual beds undergo a transformation from one facies to the next in the lateral depositional continuum at about the same lateral position. Collectively, these observations suggest that beds within a discrete multi-bed stratal unit are more or less texturally self-similar and therefore deposited from flows with similar hydraulic and compositional character, albeit exhibiting a minor but nevertheless progressive upward decrease in flow energy. This spatial and temporal regularity is argued to have been generated by multiple avulsion-related surges of a single, gradually waning turbidity current. Importantly, the time between the successive surges is estimated to have been of sufficient duration to allow for the emplacement of the traction-structured sandstone and overlying mud cap. Furthermore, the upward stacking at successive stratal units is dominated by side-stepping with minor back-stepping in the WSG compared with mostly back-stepping in the CF. Overall, the initiation, back-stepping, and side-stepping of stratal units are interpreted to be related to a combination of knickpoint migration and local topographical steering of the flows, which continued until the supply of mud from local seafloor erosion became exhausted.

ACKNOWLEDGMENTS

We thank journal reviewer Marco Patacci, an anonymous reviewer, and Associate Editor Andrea Fildani for their helpful suggestions and insights on an earlier version of this manuscript. Funding for this research has been generously provided by members of the Windermere Consortium (Occidental Petroleum [OXY] and Cenovus [Husky Energy]), Husky Energy Fellowships in Sedimentology and Petroleum Geology to Ningthoujam and Wearmouth, and a Natural Sciences and Engineering Research Council of Canada (NSERC) Discovery Grant to Arnott.

REFERENCES CITED

Aalto, K.R., 1971, Glacial marine sedimentation and stratigraphy of the Toby Conglomerate (Upper Proterozoic), southeastern British Columbia, northwestern Idaho and Northeastern Washington: Canadian Journal of Earth Sciences, v. 8, p. 753–787, https://doi.org/10.1139/e71-073.

Angus, K., Arnott, R.W.C., and Terlaky, V., 2019, Lateral and vertical juxtaposition of matrix-rich and matrix-poor lithologies caused by particle settling in mixed mud–sand deep-marine sediment suspensions: Sedimentology, v. 66, p. 940–962, https://doi.org/10.1111/sed.12523.

Armitage, D.A., McHargue, T., Fildani, A., and Graham, S.A., 2012, Postavulsion channel evolution: Niger Delta continental slope: AAPG Bulletin, v. 96, p. 823–843, https://doi.org/10.1306/09131110189.

Arnott, R.W.C., 2007a, Stratal architecture and origin of lateral accretion deposits (LADs) and conterminuous inner-bank levee deposits in a base-of-slope sinuous channel, lower Isaac Formation (Neoproterozoic), East-Central British Columbia, Canada: Marine and Petroleum Geology, v. 24, p. 515–528, https://doi.org/10.1016/j.marpetgeo.2007.01.006.

Arnott, R.W.C., 2007b, Stratigraphic architecture and depositional processes of a proximal crevasse splay and genetically related, sinuous channel fill, Isaac Formation, British Columbia, Canada, *in* Nilsen, T.H., Shew, R.D., Steffens, G.S., and Studlick, J.R.J., eds., Atlas of Deep-Water Outcrops: American Association of Petroleum Geologists Studies in Geology 56, CD-ROM chapter 128.

Arnott, R.W.C., Tilston, M., Fraino, P., Navarro, L., Dumouchel, G., and Miklovich, N., 2021, Laterally accreting sinuous channels and their deposits: The Goldilocks of deep-water slope systems: Journal of Sedimentary Research, v. 91, p. 451–463, https://doi.org/10.2110/jsr.2020.144.

Awadallah, S.A.M., 2002, Architecture and depositional history of the lower Cloridorme Formation, Gaspé Peninsula, Québec, Canada [Ph.D. thesis]: St. John's, Memorial University of Newfoundland, 376 p.

Azpiroz-Zabala, M., Cartigny, M.J.B., Talling, P.J., Parsons, D.R., Sumner, E.J., Clare, M.A., Simmons, S.M., Cooper, C., and Pope, E.L., 2017, Newly recognized turbidity current structure can explain prolonged flushing of submarine canyons: Science Advances, v. 3, https://doi.org/10.1126/sciadv.1700200.

Baas, J.H., Best, J.L., and Peakall, J., 2011, Depositional processes, bedform development and hybrid bed formation in rapidly decelerated cohesive (mud–sand) sediment flows: Sedimentology, v. 58, p. 1953–1987, https://doi.org/10.1111/j.1365-3091.2011.01247.x.

Baltzer, A., Cochonat, P., and Piper, D.J.W., 1994, In situ geotechnical characterization of sediments on the Nova Scotian Slope, eastern Canadian continental margin: Marine Geology, v. 120, p. 291–308, https://doi.org/10.1016/0025-3227(94)90063-9.

Barker, S.P., Haughton, P.D., McCaffrey, W.D., Archer, S.G., and Hakes, B., 2008, Development of rheological heterogeneity in clay-rich high-density turbidity currents: Aptian Britannia Sandstone Member, UK continental shelf: Journal of Sedimentary Research, v. 78, p. 45–68, https://doi.org/10.2110/jsr.2008.014.

Beeden, D.R., 1983, Sedimentology of some turbidites and related rocks from the Cloridorme Group, Ordovician, Quebec [M.S. thesis]: Hamilton, Ontario, McMaster University, 229 p.

Bennett, H.R., O'Brien, N.R., and Hulbert, M.H., 1992, Determinants of clay and shale microfabric signatures: Processes and mechanisms, *in* Bennett, H.R., Bryant, W.R., Hulbert, M.H., eds., Microstructure of Fine-Grained Sediments: From Mud to Shale: New York, Springer-Verlag, p. 5–32, https://doi.org/10.1007/978-1-4612-4428-8_2.

Best, J.L., Kostaschuk, R.A., Peakall, J., Villard, P.V., and Franklin, M., 2005, Whole flow field dynamics and velocity pulsing within natural sediment-laden underflows: Geology, v. 33, p. 765–768, https://doi.org/10.1130/G21516.1.

Bhaskar, P.V., and Bhosle, N.B., 2005, Microbial extracellular polymeric substances in marine biogeochemical processes: Current Science, v. 88, p. 45–53.

Bouma, A.H., 1962, Sedimentology of Some Flysch Deposits: A Graphic Approach to Facies Interpretation: Amsterdam, Elsevier, 168 p.

Burgess, P.M., Masiero, I., Toby, S.C., and Duller, R.A., 2019, A big fan of signals? Exploring autogenic and allogenic process and product in a numerical stratigraphic forward model of submarine-fan development: Journal of Sedimentary Research, v. 89, p. 1–12, https://doi.org/10.2110/jsr.2019.3.

Campbell, R.B., Mountjoy, E.W., and Young, F.G., 1973, Geology of McBride map-area, British Columbia (93H): Geological Survey of Canada Paper 72-35, 104 p., 3 sheets, scale 1:250,000, https://doi.org/10.4095/103468.

Canals, M., Lastras, G., Urgeles, R., Casamor, J.L., Mienert, J., Cattaneo, A., De Batist, M., Haflidason, H., Imbo, Y., Laberg, J.S., Locat, J., Long, D., Longva, O., Masson, D.G., Sultan, N., Trincardi, F., and Bryn, P., 2004, Slope failure dynamics and impacts from seafloor and shallow sub-seafloor geophysical data: Case studies from the COSTA project: Marine Geology, v. 213, p. 9–72, https://doi.org/10.1016/j.margeo.2004.10.001.

Cantelli, A., Pirmez, C., Johnson, S., and Parker, G., 2011, Morphodynamic and stratigraphic evolution of self-channelized subaqueous fans emplaced by turbidity currents: Journal of Sedimentary Research, v. 81, p. 233–247, https://doi.org/10.2110/jsr.2011.20.

Carr, T.R., 1982, Log-linear models, Markov chains and cyclic sedimentation: Journal of Sedimentary Research, v. 52, p. 905–912, https://doi.org/10.1306/212F808A-2B24-11D7-8648000102C1865D.

Cartigny, M.J.B., Eggenhuisen, J.T., Hansen, E.W.M., and Postma, G., 2013, Concentration-dependent flow stratification in experimental high-density turbidity currents and their relevance to turbidite facies models: Journal of Sedimentary Research, v. 83, p. 1046–1064, https://doi.org/10.2110/jsr.2013.71.

Carvajal, C., Paull, C.K., Caress, D.W., Fildani, A., Lundsten, E., Anderson, K., Maier, K.L., McGann, M., Gwiazda, R., and Herguera, J.C., 2017, Unraveling the channel–lobe transition zone with high-resolution AUV bathymetry: Navy Fan, offshore Baja California, Mexico: Journal of Sedimentary Research, v. 87, p. 1049–1059, https://doi.org/10.2110/jsr.2017.58.

Cunningham, C.M., and Arnott, R.W.C., 2021, Systematic organization of thin-bedded turbidites in ancient deep-marine levees: Possible evidence of rhythmic pulsing in turbidity currents: Journal of Sedimentary Research, v. 91, p. 1257–1274, https://doi.org/10.2110/jsr.2021.003.

Dade, W.B., Davis, J.D., Nichols, P.D., Nowell, A.R.M., Thistle, D., Trexler, M.B., White, D.C., and Davis, J.D., 1990, Effects of bacterial exopolymer adhesion on the entrainment of sand: Geomicrobiology Journal, v. 8, p. 1–16, https://doi.org/10.1080/01490459009377874.

Dade, W.B., Self, R.L., Pellerin, N.B., Moffet, A., Jumars, P.A., and Nowell, A.R.M., 1996, The effects of bacteria on the flow behavior of clay-seawater suspensions: Journal of Sedimentary Research, v. 66, p. 39–42, https://doi.org/10.1306/D42682A7-2B26-11D7-8648000102C1865D.

Dai, H.H., 2008, Analysis and modeling of plunging flows [Ph.D. thesis]: Urbana, University of Illinois Urbana-Champaign, 121 p.

Davarpanah Jazi, S., and Wells, M.G., 2016, Enhanced sedimentation beneath particle-laden flows in lakes and the ocean due to double-diffusive convection: Geophysical Research Letters, v. 43, p. 10,883–10,890, https://doi.org/10.1002/2016GL069547.

Davarpanah Jazi, S., and Wells, M.G., 2020, Dynamics of settling-driven convection beneath a sediment-laden buoyant overflow: Implications for the length-scale of deposition in lakes and the coastal ocean: Sedimentology, v. 67, p. 699–720, https://doi.org/10.1111/sed.12660.

Davis, C., Haughton, P., McCaffrey, W., Scott, E., Hogg, N., and Kitching, D., 2009, Character and distribution of hybrid sediment gravity flow deposits from the outer Forties Fan, Palaeocene Central North Sea, UKCS: Marine and Petroleum Geology, v. 26, p. 1919–1939, https://doi.org/10.1016/j.marpetgeo.2009.02.015.

Davis, J.C., 1986, Statistics and Data Analysis in Geology (2nd edition): New York, John Wiley and Sons, 646 p.

Deptuck, M.E., Piper, D.J.W., Savoye, B., and Gervais, A., 2008, Dimensions and architecture of late Pleistocene submarine lobes off the northern margin of East Corsica: Sedimentology, v. 55, p. 869–898, https://doi.org/10.1111/j.1365-3091.2007.00926.x.

Duringer, P., Paicheler, J.C., and Schneider, J.L., 1991, Un courant d'eau continu peut-il générer des turbidites? Résultats d'expérimentations analogiques: Marine Geology, v. 99, p. 231–246, https://doi.org/10.1016/0025-3227(91)90093-J.

Ehlers, C.J., Chen, J., Roberts, H.H., and Lee, Y.C., 2005, The origin of near-seafloor "crust zones" in deepwater, *in* Gourvenec, S., and Cassidy, M., eds., Frontiers in Offshore Geotechnics, ISFOG 2005: Proceedings of the 1st International Symposium on Frontiers in Offshore Geotechnics, University of Western Australia, Perth, 19–21 September 2005: London, Taylor & Francis, p. 927–934.

Enos, P., 1969, Anatomy of a flysch: Journal of Sedimentary Petrology, v. 39, p. 680–723, https://doi.org/10.1306/74D71CF8-2B21-11D7-8648000102C1865D.

Ferguson, R.A., Kane, I.A., Eggenhuisen, J.T., Pohl, F., Tilston, M., Spychala, Y.T., and Brunt, R.L., 2020, Entangled external and internal controls on submarine fan evolution: An experimental perspective: The Depositional Record, v. 6, p. 605–624, https://doi.org/10.1002/dep2.109.

Fernandez, R.L., Cantelli, A., Pirmez, C., Sequeiros, O., and Parker, G., 2014, Growth patterns of subaqueous depositional channel lobe systems developed over a basement with a downdip break in slope: Laboratory experiments: Journal of Sedimentary Research, v. 84, p. 168–182, https://doi.org/10.2110/jsr.2014.10.

Fildani, A., Normark, W.R., Kostic, S., and Parker, G., 2006, Channel formation by flow stripping: Large-scale scour features along the Monterey East Channel and their relation to sediment waves: Sedimentology, v. 53, p. 1265–1287, https://doi.org/10.1111/j.1365-3091.2006.00812.x.

Fildani, A., Hubbard, S.M., Covault, J.A., Maier, K.L., Romans, B.W., Traer, M., and Rowland, J.C., 2013, Erosion at inception of deep-sea channels: Marine and Petroleum Geology, v. 41, p. 48–61, https://doi.org/10.1016/j.marpetgeo.2012.03.006.

Fildani, A., Clark, J., Covault, J.A., Power, B., Romans, B.W., and Aiello, I.W., 2018, Muddy sand and sandy mud on the distal Mississippi fan: Implications for lobe depositional processes: Geosphere, v. 14, p. 1051–1066, https://doi.org/10.1130/GES01580.1.

Fonnesu, M., Haughton, P., Felletti, F., and McCaffrey, W., 2015, Short length-scale variability of hybrid event beds and its applied significance: Marine and Petroleum Geology, v. 67, p. 583–603, https://doi.org/10.1016/j.marpetgeo.2015.03.028.

Fonnesu, M., Patacci, M., Haughton, P.D.W., Felletti, F., and McCaffrey, W.D., 2016, Hybrid event beds generated by local substrate delamination on a confined-basin floor: Journal of Sedimentary Research, v. 86, p. 929–943, https://doi.org/10.2110/jsr.2016.58.

Fonnesu, M., Felletti, F., Haughton, P.D.W., Patacci, M., and McCaffrey, W.D., 2018, Hybrid event bed character and distribution linked to turbidite system sub-environments: The North Apennine Gottero Sandstone (north-west Italy): Sedimentology, v. 65, p. 151–190, https://doi.org/10.1111/sed.12376.

Gervais, A., Savoye, B., Mulder, T., and Gonthier, E., 2006, Sandy modern turbidite lobes: A new insight from high resolution seismic data: Marine and Petroleum Geology, v. 23, p. 485–502, https://doi.org/10.1016/j.marpetgeo.2005.10.006.

Haughton, P.D.W., 1994, Deposits of deflected and ponded turbidity currents, Sorbas Basin, Southeast Spain: Journal of Sedimentary Research, v. 64, p. 233–246, https://doi.org/10.1306/D4267D6B-2B26-11D7-8648000102C1865D.

Haughton, P.D.W., Barker, S.P., and McCaffrey, W.D., 2003, "Linked" debrites in sand-rich turbidite systems—Origin and significance: Sedimentology, v. 50, p. 459–482, https://doi.org/10.1046/j.1365-3091.2003.00560.x.

Haughton, P., Davis, C., McCaffrey, W., and Barker, S., 2009, Hybrid sediment gravity flow deposits—Classification, origin and significance: Marine and Petroleum Geology, v. 26, p. 1900–1918, https://doi.org/10.1016/j.marpetgeo.2009.02.012.

Hiscott, R.N., 1984, Ophiolitic source rocks for Taconic-age flysch: Trace-element evidence: Geological Society of America Bulletin, v. 95, p. 1261–1267, https://doi.org/10.1130/0016-7606(1984)95<1261:OSRFTF>2.0.CO;2.

Hiscott, R.N., Pickering, K.T., and Beeden, D.R., 1986, Progressive filling of a confined Middle Ordovician foreland basin associated with the Taconic Orogeny, Quebec, Canada, *in* Allen, P.A., and Homewood, P., eds., Foreland Basins: International Association of Sedimentologists Special Publication 8: Oxford, UK, Wiley, p. 307–325, https://doi.org/10.1002/9781444303810.ch17.

Ho, V.L., Dorrell, R.M., Keevil, G.M., Burns, A.D., and McCaffrey, W.D., 2018a, Pulse propagation in turbidity currents: Sedimentology, v. 65, p. 620–637, https://doi.org/10.1111/sed.12397.

Ho, V.L., Dorrell, R.M., Keevil, G.M., Burns, A.D., and McCaffrey, W.D., 2018b, Scaling analysis of multipulsed turbidity current evolution with application to turbidite interpretation: Journal of Geophysical Research: Oceans, v. 123, p. 3668–3684, https://doi.org/10.1029/2017JC013463.

Hodgson, D.M., 2009, Distribution and origin of hybrid beds in sand-rich submarine fans of the Tanqua depocentre, Karoo Basin, South Africa: Marine and Petroleum Geology, v. 26, p. 1940–1956, https://doi.org/10.1016/j.marpetgeo.2009.02.011.

Hodgson, D.M., Flint, S.S., Hodgetts, D., Drinkwater, N.J., Johannessen, E.P., and Luthi, S.M., 2006, Stratigraphic evolution of fine-grained submarine fan systems, Tanqua depocenter, Karoo Basin, South Africa: Journal of Sedimentary Research, v. 76, p. 20–40, https://doi.org/10.2110/jsr.2006.03.

Hoyal, D.C., Bursik, M.I., and Atkinson, J.F., 1999, Settling-driven convection: A mechanism of sedimentation from stratified fluids: Journal of Geophysical Research, v. 104, p. 7953–7966, https://doi.org/10.1029/1998JC900065.

Hughes Clarke, J.E., 2016, First wide-angle view of channelized turbidity currents links migrating cyclic steps to flow characteristics: Nature Communications, v. 7, https://doi.org/10.1038/ncomms11896.

Jegou, I., Savoye, B., Pirmez, C., and Droz, L., 2008, Channel-mouth lobe complex of the recent Amazon Fan: The missing piece: Marine Geology, v. 252, p. 62–77, https://doi.org/10.1016/j.margeo.2008.03.004.

Jiang, W.T., and Peacor, D.R., 1994, Prograde transitions of corrensite and chlorite in low-grade pelitic rocks from the Gaspé Peninsula, Quebec: Clays and Clay Minerals, v. 42, p. 497–517, https://doi.org/10.1346/CCMN.1994.0420501.

Jobe, Z.R., Sylvester, Z., Howes, N., Pirmez, C., Parker, A., Cantelli, A., Smith, R., Wolinsky, M.A., O'Byrne, C., Slowey, N., and Prather, B., 2017, High-resolution, millennial-scale patterns of bed compensation on a sand-rich intraslope submarine fan, western Niger Delta slope: Geological Society of America Bulletin, v. 129, p. 23–37, https://doi.org/10.1130/B31440.1.

Kane, I.A., and Pontén, A.S.M., 2012, Submarine transitional flow deposits in the Paleogene Gulf of Mexico: Geology, v. 40, p. 1119–1122, https://doi.org/10.1130/G33410.1.

Kane, I.A., Pontén, A.S.M., Vangdal, B., Eggenhuisen, J.T., Hodgson, D.M., and Spychala, Y.T., 2017, The stratigraphic record and processes of turbidity current transformation across deep-marine lobes: Sedimentology, v. 64, p. 1236–1273, https://doi.org/10.1111/sed.12346.

Kelly, R.W., Dorrell, R.M., Burns, A.D., and McCaffrey, W.D., 2019, The structure and entrainment characteristics of partially confined gravity currents: Journal of Geophysical Research: Oceans, v. 124, p. 2110–2125, https://doi.org/10.1029/2018JC014042.

Khan, Z.A., and Arnott, R.W.C., 2011, Stratal attributes and evolution of asymmetric inner- and outer-bend levee deposits associated with an ancient deep-water channel-levee complex within the Isaac Formation, southern Canada: Marine and Petroleum Geology, v. 28, p. 824–842, https://doi.org/10.1016/j.marpetgeo.2010.07.009.

Khripounoff, A., Crassous, P., Lo Bue, N., Dennielou, B., and Silva Jacinto, R., 2012, Different types of sediment gravity flows detected in the Var submarine canyon (northwestern Mediterranean Sea): Progress in Oceanography, v. 106, p. 138–153, https://doi.org/10.1016/j.pocean.2012.09.001.

Kneller, B., and Buckee, C., 2000, The structure and fluid mechanics of turbidity currents: A review of some recent studies and their geological implications: Sedimentology, v. 47, p. 62–94, https://doi.org/10.1046/j.1365-3091.2000.047s1062.x.

Koo, W.M., Mohrig, D., Buttles, J., Sturmer, D., Pontén, A., and Hess, T., 2020, Sand–mud couplets deposited by spontaneous remobilization of subaqueous transitional flows: Sedimentology, v. 67, p. 78–95, https://doi.org/10.1111/sed.12625.

Kostaschuk, R., Nasr-Azadani, M.M., Meiburg, E., Wei, T.Y., Chen, Z.Y., Negretti, M.E., Best, J., Peakall, J., and Parsons, D.R., 2018, On the causes of pulsing in continuous turbidity currents:

Journal of Geophysical Research: Earth Surface, v. 123, p. 2827–2843, https://doi.org/10.1029/2018JF004719.
Krumbein, W.C., 1968, Statistical models in sedimentology: Sedimentology, v. 10, p. 7–23, https://doi.org/10.1111/j.1365-3091.1968.tb01908.x.
Kuo, M., and Bolton, M., 2008, Preliminary investigation into the influence of bacteria in marine sediments, *in* Proceedings, 1st International Conference on Bio-Geo-Civil Engineering, Delft, Netherlands, p. 76–81.
Kuo, M., and Bolton, M., 2013, The nature and origin of deep ocean clay crust from the Gulf of Guinea: Géotechnique, v. 63, p. 500–509, https://doi.org/10.1680/geot.10.P.012.
Larue, D.K., and Provine, K.G., 1988, Vacillatory turbidites, Barbados: Sedimentary Geology, v. 57, p. 211–219, https://doi.org/10.1016/0037-0738(88)90028-0.
Lehrmann, D.J., and Goldhammer, R.K., 1999, Secular variation in parasequence and facies stacking patterns of platform carbonates: A guide to application of stacking-patterns analysis in strata of diverse ages and settings, *in* Harris, P.M., Saller, A.H., and Simo, J.A., eds., Advances in Carbonate Sequence Stratigraphy: Application to Reservoirs, Outcrops and Models: SEPM (Society for Sedimentary Geology) Special Publication 63, p. 187–225, https://doi.org/10.2110/pec.99.11.0187.
Liu, J.T., Wang, Y.H., Yang, R.J., Hsu, R.T., Kao, S.J., Lin, H.L., and Kuo, F.H., 2012, Cyclone-induced hyperpycnal turbidity currents in a submarine canyon: Journal of Geophysical Research, v. 117, C04033, https://doi.org/10.1029/2011JC007630.
Lowe, D.R., 1982, Sediment gravity flows: II, Depositional models with special reference to the deposits of high-density turbidity currents: Journal of Sedimentary Petrology, v. 52, p. 279–297, https://doi.org/10.1306/212F7F31-2B24-11D7-8648000102C1865D.
Lowe, D.R., and Guy, M., 2000, Slurry-flow deposits in the Britannia Formation (Lower Cretaceous), North Sea: A new perspective on the turbidity current and debris flow problem: Sedimentology, v. 47, p. 31–70, https://doi.org/10.1046/j.1365-3091.2000.00276.x.
Maier, K.L., Paull, C.K., Caress, D.W., Anderson, K., Nieminski, N.M., Lundsten, E., Erwin, B.E., Gwiazda, R., and Fildani, A., 2020, Submarine-fan development revealed by integrated high-resolution datasets from La Jolla Fan, offshore California, USA: Journal of Sedimentary Research, v. 90, p. 468–479, https://doi.org/10.2110/jsr.2020.22.
Marsset, T., Droz, L., Dennielou, B., and Pichon, E., 2009, Cycles in the architecture of the Quaternary Zaire turbidite system: A possible link with climate, *in* Kneller, B., Martinsen, O.J., and McCaffrey, B., eds., External Controls on Deep-Water Depositional Systems: SEPM (Society for Sedimentary Geology) Special Publication 92, p. 89–106, https://doi.org/10.2110/sepmsp.092.089.
McAnally, W.H., Friedrichs, C., Hamilton, D., Hayter, E., Shrestha, P., Rodriguez, H., Sheremet, A., and Teeter, A., 2007, Management of fluid mud in estuaries, bays, and lakes. I: Present state of understanding on character and behavior: Journal of Hydraulic Engineering, v. 133, p. 9–22, https://doi.org/10.1061/(ASCE)0733-9429(2007)133:1(9).
McMechan, M.E., 2015, The Neoproterozoic succession of the central Rocky Mountains, Canada: Bulletin of Canadian Petroleum Geology, v. 63, p. 243–273, https://doi.org/10.2113/gscpgbull.63.3.243.
Meadows, A., and Meadows, P.S., 1994, Bioturbation in deep sea Pacific sediments: Journal of the Geological Society, v. 151, p. 361–375, https://doi.org/10.1144/gsjgs.151.2.0361.
Menczel, A., and Kostaschuk, R., 2013, Interfacial waves as coherent flow structures associated with continuous turbidity currents: Lillooet Lake, Canada, *in* Venditti, J.G., Best, J.L., Church, M., and Hardy, R.J., eds., Coherent Flow Structures at Earth's Surface: Chichester, UK, Wiley, p. 371–383.
Middleton, G.V., 1966, Experiments on density and turbidity currents: I. Motion of the head: Canadian Journal of Earth Sciences, v. 3, p. 523–546, https://doi.org/10.1139/e66-038.
Mountjoy, E.W., and Aitken, J.D., 1963, Early Cambrian and late Precambrian paleocurrents, Banff and Jasper National Parks: Bulletin of Canadian Petroleum Geology, v. 11, p. 161–168.
Nakajima, T., and Kanai, Y., 2000, Sedimentary features of seismoturbidites triggered by the 1983 and older historical earthquakes in the eastern margin of the Japan Sea: Sedimentary Geology, v. 135, p. 1–19, https://doi.org/10.1016/S0037-0738(00)00059-2.
Navarro, L., and Arnott, R.W.C., 2020, Stratigraphic record in the transition from basin floor to continental slope sedimentation in the ancient passive-margin Windermere turbidite system: Sedimentology, v. 67, p. 1710–1749, https://doi.org/10.1111/sed.12676.
Ningthoujam, J., Wearmouth, C., and Arnott, R.W.C., 2022, Stratal characteristic and depositional origin of two-part (mud-poor overlain by mud-rich) and associated deep-water strata: Components in a lateral depositional continuum related to particle settling in negligibly sheared mud-rich suspensions: Journal of Sedimentary Research, v. 92, p. 503–529, https://doi.org/10.2110/jsr.2021.053.
O'Byrne, C.J., Barton, M.D., Steffens, G.S., Pirmez, C., and Buergisser, H., 2007, Architecture of a laterally migrating channel complex: Channel 4, Isaac Formation, Windermere Supergroup, Castle Creek north, British Columbia, Canada, *in* Nilsen, T.H., Shew, R.D., Steffens, G.S., and Studlick, J.R.J., eds., Atlas of Deep-Water Outcrops: American Association of Petroleum Geologists Studies in Geology 56, p. 115–118.
Parkash, B., and Middleton, G.V., 1970, Downcurrent textural changes in Ordovician turbidite greywackes: Sedimentology, v. 14, p. 259–293, https://doi.org/10.1111/j.1365-3091.1970.tb00195.x.
Parkes, R.J., Cragg, B.A., and Wellsbury, P., 2000, Recent studies on bacterial populations and processes in subseafloor sediments: A review: Hydrogeology Journal, v. 8, p. 11–28, https://doi.org/10.1007/PL00010971.
Parsons, J.D., Bush, J.W.M., and Syvitski, J.P.M., 2001, Hyperpycnal plume formation from riverine outflows with small sediment concentrations: Sedimentology, v. 48, p. 465–478, https://doi.org/10.1046/j.1365-3091.2001.00384.x.
Patacci, M., Haughton, P.D.W., and McCaffrey, W.D., 2014, Rheological complexity in sediment gravity flows forced to decelerate against a confining slope, Braux, SE France: Journal of Sedimentary Research, v. 84, p. 270–277, https://doi.org/10.2110/jsr.2014.26.
Pickering, K.T., 1979, Possible retrogressive flow slide deposits from the Kongsfjord Formation: A Precambrian submarine fan, Finnmark, N. Norway: Sedimentology, v. 26, p. 295–306, https://doi.org/10.1111/j.1365-3091.1979.tb00356.x.
Pickering, K.T., and Hiscott, R.N., 1985, Contained (reflected) turbidity currents from the Middle Ordovician Cloridorme Formation, Quebec, Canada: An alternative to the antidune hypothesis: Sedimentology, v. 32, p. 373–394, https://doi.org/10.1111/j.1365-3091.1985.tb00518.x.
Pierce, C.S., Haughton, P.D., Shannon, P.M., Pulham, A.J., Barker, S.P., and Martinsen, O.J., 2018, Variable character and diverse origin of hybrid event beds in a sandy submarine fan system, Pennsylvanian Ross Sandstone Formation, western Ireland: Sedimentology, v. 65, p. 952–992, https://doi.org/10.1111/sed.12412.
Piper, D.J.W., Cochonat, P., and Morrison, M.L., 1999, The sequence of events around the epicentre of the 1929 Grand Banks earthquake: Initiation of debris flows and turbidity current inferred from sidescan sonar: Sedimentology, v. 46, p. 79–97, https://doi.org/10.1046/j.1365-3091.1999.00204.x.
Pirmez, C., Hiscott, R.N., and Kronen, J.K., Jr., 1997, Sandy turbidite successions at the base of channel-levee systems of the Amazon Fan revealed by FMS logs and cores: Unraveling the facies architecture of large submarine fans, *in* Flood, R.D., Piper, D.J.W., Klaus, A., and Peterson, L.C., eds., Proceedings of the Ocean Drilling Program, Scientific Results, Volume 155: College Station, Texas, Ocean Drilling Program, p. 7–22, https://doi.org/10.2973/odp.proc.sr.155.201.1997.
Pirmez, C., Beaubouef, R.T., Friedmann, S.J., and Mohrig, D.C., 2000, Equilibrium profile and baselevel in submarine channels: Examples from Late Pleistocene systems and implications for the architecture of deepwater reservoirs, *in* Weimer, P., Slatt, R.M., Coleman, J., Rosen, N.C., Nelson, H., Bouma, A.H., Styzen, M.J., and Lawrence, D.T., eds., Deep-Water Reservoirs of the World: Gulf Coast Section of the Society of Economic Paleontologists and Mineralogists Foundation 20th Annual Research Conference, p. 782–805, https://doi.org/10.5724/gcs.00.15.0782.
Pratson, L.E., Imran, J., Parker, G., Syvitski, J.P.M., and Hutton, E., 2000, Debris flows vs. turbidity currents: A modeling comparison of their dynamics and deposits, *in* Bouma, A.H., and Stone, C.G., eds., Fine-Grained Turbidite Systems: American Association of Petroleum Geologists Memoir 72, p. 57–72, https://doi.org/10.1306/M72703C6.
Prélat, A., Hodgson, D.M., and Flint, S.S., 2009, Evolution, architecture and hierarchy of distributary deep-water deposits: A high-resolution outcrop investigation from the Permian Karoo Basin, South Africa: Sedimentology, v. 56, p. 2132–2154, https://doi.org/10.1111/j.1365-3091.2009.01073.x.
Riva, J., 1968, Graptolite faunas from the Middle Ordovician of the Gaspé north shore: Naturaliste Canadien, v. 93, p. 1379–1400.
Romans, B.W., Normark, W.R., McGann, M.M., Covault, J.A., and Graham, S.A., 2009, Coarse-grained sediment delivery and distribution in the Holocene Santa Monica Basin, California: Implications for evaluating source-to-sink flux at millennial time scales: Geological Society of America Bulletin, v. 121, p. 1394–1408, https://doi.org/10.1130/B26393.1.
Ross, G.M., and Arnott, R.W.C., 2007, Regional geology of the Windermere Supergroup, southern Canadian Cordillera and stratigraphic setting of the Castle Creek study area, Canada,

in Nilsen, T.H., Shew, R.D., Steffens, G.S., and Studlick, J.R.J., eds., Atlas of Deep-Water Outcrops: American Association of Petroleum Geologists Studies in Geology 56, CD-ROM chapter 124.

Ross, G.M., Bloch, J.D., and Krouse, H.R., 1995, Neoproterozoic strata of the southern Canadian Cordillera and the isotopic evolution of seawater sulfate: Precambrian Research, v. 73, p. 71–99, https://doi.org/10.1016/0301-9268(94)00072-Y.

Schwarz, E., and Arnott, R.W.C., 2007, Anatomy and evolution of a slope channel-complex set (Neoproterozoic Isaac Formation, Windermere Supergroup, southern Canadian Cordillera): Implications for reservoir characterization: Journal of Sedimentary Research, v. 77, p. 89–109, https://doi.org/10.2110/jsr.2007.015.

Schwarzacher, W., 1975, Markov chains, *in* Sedimentation Models and Quantitative Stratigraphy: Amsterdam, Elsevier Scientific Publishing, Developments in Sedimentology, v. 19, p. 91–121, https://doi.org/10.1016/S0070-4571(08)70371-6.

Shepard, F.P., Marshall, N.F., and McLoughlin, P.A., 1975, Pulsating turbidity currents with relationship to high swell and high tides: Nature, v. 258, p. 704–706, https://doi.org/10.1038/258704a0.

Skempton, A.W., 1969, The consolidation of clays by gravitational compaction: Quarterly Journal of the Geological Society of London, v. 125, p. 373–411, https://doi.org/10.1144/gsjgs.125.1.0373.

Southern, S.J., Patacci, M., Felletti, F., and McCaffrey, W.D., 2015, Influence of flow containment and substrate entrainment upon sandy hybrid event beds containing a co-genetic mud-clast-rich division: Sedimentary Geology, v. 321, p. 105–122, https://doi.org/10.1016/j.sedgeo.2015.03.006.

Spychala, Y.T., Hodgson, D.M., Prélat, A., Kane, I.A., Flint, S.S., and Mountney, N.P., 2017a, Frontal and lateral submarine lobe fringes: Comparing sedimentary facies, architecture and flow processes: Journal of Sedimentary Research, v. 87, p. 75–96, https://doi.org/10.2110/jsr.2017.2.

Spychala, Y.T., Hodgson, D.M., and Lee, D.R., 2017b, Autogenic controls on hybrid bed distribution in submarine lobe complexes: Marine and Petroleum Geology, v. 88, p. 1078–1093, https://doi.org/10.1016/j.marpetgeo.2017.09.005.

St. Julien, P., and Hubert, C., 1975, Evolution of the Taconian orogen in the Quebec Appalachians: American Journal of Science, v. 275, p. 337–362.

Stewart, J.H., 1972, Initial deposits in the Cordilleran geosyncline: Evidence of a late Precambrian (<850 m.y.) continental separation: Geological Society of America Bulletin, v. 83, p. 1345–1360, https://doi.org/10.1130/0016-7606(1972)83[1345:IDITCG]2.0.CO;2.

Straub, K.M., Mohrig, D., McElroy, B., Buttles, J., and Pirmez, C., 2008, Interactions between turbidity currents and topography in aggrading sinuous submarine channels: A laboratory study: Geological Society of America Bulletin, v. 120, p. 368–385, https://doi.org/10.1130/B25983.1.

Talling, P.J., 2013, Hybrid submarine flows comprising turbidity current and cohesive debris flow: Deposits, theoretical and experimental analyses, and generalized models: Geosphere, v. 9, p. 460–488, https://doi.org/10.1130/GES00793.1.

Talling, P.J., Amy, L.A., Wynn, R.B., Peakall, J., and Robinson, M., 2004, Beds comprising debrite sandwiched within co-genetic turbidite: Origin and widespread occurrence in distal depositional environments: Sedimentology, v. 51, p. 163–194, https://doi.org/10.1111/j.1365-3091.2004.00617.x.

Terlaky, V., and Arnott, R.W.C., 2014, Matrix-rich and associated matrix-poor sandstones: Avulsion splays in slope and basin-floor strata: Sedimentology, v. 61, p. 1175–1197, https://doi.org/10.1111/sed.12096.

Terlaky, V., and Arnott, R.W.C., 2016, The control of terminal-splay sedimentation on depositional patterns and stratigraphic evolution in avulsion-dominated, unconfined, deep-marine basin-floor systems: Journal of Sedimentary Research, v. 86, p. 786–799, https://doi.org/10.2110/jsr.2016.51.

Terlaky, V., Rocheleau, J., and Arnott, R.W.C., 2016, Stratal composition and stratigraphic organization of stratal elements in an ancient deep-marine basin-floor succession, Neoproterozoic Windermere Supergroup, British Columbia, Canada: Sedimentology, v. 63, p. 136–175, https://doi.org/10.1111/sed.12222.

Tolhurst, T.J., Gust, G., and Paterson, D.M., 2002, The influence of an extracellular polymeric substance (EPS) on cohesive sediment stability: Proceedings in Marine Science, v. 5, p. 409–425, https://doi.org/10.1016/S1568-2692(02)80030-4.

Twichell, D.C., Kenyon, N.H., Parson, L.M., and McGregor, B.A., 1991, Depositional patterns of the Mississippi Fan surface: Evidence from GLORIA II and high-resolution seismic profiles, *in* Weimer, P., and Link, M.H., eds., Seismic Facies and Sedimentary Processes of Submarine Fans and Turbidite Systems: New York, Springer, p. 349–363, https://doi.org/10.1007/978-1-4684-8276-8_19.

Vittori, J., Morash, A., Savoye, B., Marsset, T., Lopez, M., Droz, L., and Cremer, M., 2000, The Quaternary Congo deep-sea fan: Preliminary results on reservoir complexity in turbiditic systems using 2D high resolution seismic and multibeam data, *in* Weimer, P., Slatt, R.M., Coleman, J., Rosen, N.C., Nelson, H., Bouma, A.H., Styzen, M.J., and Lawrence, D.T., eds., Deep-Water Reservoirs of the World: Gulf Coast Section Society of Economic Paleontologists and Mineralogists Foundation 20th Annual Research Conference, p. 1045–1058, https://doi.org/10.5724/gcs.00.15.1045.

Warren, M.J., 1997, Crustal extension and subsequent crustal thickening along the Cordilleran rifted margin of ancestral North America, western Purcell Mountains, southeastern British Columbia [Ph.D. thesis]: Kingston, Ontario, Queen's University, 361 p.

Wearmouth, C., 2018, Spatial, temporal and physical origin of matrix-poor to matrix-rich sandstones, Neoproterozoic Windermere Supergroup, British Columbia, Canada [M.S. thesis]: Ottawa, Ontario, University of Ottawa, 153 p.

Xu, J.P., Noble, M.A., and Rosenfeld, L.K., 2004, In-situ measurements of velocity structure within turbidity currents: Geophysical Research Letters, v. 31, L09311, https://doi.org/10.1029/2004GL019718.